

Optical Observations of GRO J1655-40 in Quiescence I: A Precise Mass for the Black Hole Primary

Jerome A. Orosz^{1,2} and Charles D. Bailyn^{1,3}

Department of Astronomy, Yale University, P. O. Box 208101, New Haven, CT 06520-8101

E-Mail: orosz@astro.yale.edu, bailyn@astro.yale.edu

ABSTRACT

We report photometric and spectroscopic observations of the black hole binary GRO J1655-40 in complete quiescence. In contrast to the 1995 photometry, the light curves from 1996 are almost completely dominated by ellipsoidal modulations from the secondary star. Model fits to the light curves, which take into account the temperature profile of the accretion disk and eclipse effects, yield an inclination of $i = 69.50 \pm 0.08$ deg and a mass ratio of $Q = M_1/M_2 = 2.99 \pm 0.08$. The precision of our determinations of i and Q allow us to determine the black hole mass to an accuracy of $\approx 4\%$ ($M_1 = 7.02 \pm 0.22 M_\odot$). The secondary star's mass is $M_2 = 2.34 \pm 0.12 M_\odot$. The position of the secondary on the Hertzsprung-Russell diagram is consistent with that of a $\approx 2.3 M_\odot$ star which has evolved off the main sequence and is halfway to the start of the giant branch. Using the new spectra we present an improved value of the spectroscopic period ($P = 2^d62157 \pm 0^d00015$), radial velocity semiamplitude ($K = 228.2 \pm 2.2 \text{ km s}^{-1}$), and mass function ($f(M) = 3.24 \pm 0.09 M_\odot$). Based on the new spectra of the source and spectra of several MK spectral type standards, we classify the secondary star as F3IV to F6IV. Evolutionary models suggest an average mass transfer rate for such a system of $\dot{M}_2 = 3.4 \times 10^{-9} M_\odot \text{ yr}^{-1} = 2.16 \times 10^{17} \text{ g s}^{-1}$, which is much larger than the average mass transfer rates implied in the other six transient black hole systems, but still barely below the critical mass transfer rate required for stability.

Subject headings: binaries: spectroscopic — black hole physics — X-rays: stars — stars: individual (GRO J1655-40)

¹Visiting Astronomer at Cerro Tololo Inter-American Observatory (CTIO), which is operated by the Association of Universities for Research in Astronomy Inc., under contract with the National Science Foundation.

²Present Address: Department of Astronomy & Astrophysics, The Pennsylvania State University, 525 Davey Laboratory, University Park, PA 16802

³National Young Investigator

1. Introduction

A new bright X-ray source (designated GRO J1655-40) was discovered July 27, 1994 with the Burst and Transient Source Experiment (BATSE) on board the *Compton Gamma Ray Observatory* (Zhang et al. 1994). The optical counterpart and the radio counterpart were identified soon after the announcement of the discovery by the BATSE team (Bailyn et al. 1995a; Campbell-Wilson & Hunstead 1994). About three weeks after the initial hard X-ray outburst, radio jets with apparent superluminal velocities were observed emerging from the source (Tingay et al. 1995; Hjellming & Rupen 1995), making GRO J1655-40 only the second source in our Galaxy observed to have superluminal jets and the first one to be optically identified.

Bailyn et al. (1995b) established the spectroscopic period ($2^{\text{d}}601 \pm 0^{\text{d}}027$) and the mass function ($3.16 \pm 0.15 M_{\odot}$) of the system using spectroscopic observations made during late April and early May, 1995. The photometric observations by Bailyn et al. (1995b) from early 1995 showed that GRO J1655-40 is an eclipsing binary. The light curves from March and April, 1995 all have deep triangular-shaped minima near the spectroscopic phase 0.75 (caused by an eclipse of the disk by the star) and much shallower minima near the spectroscopic phase 0.25 (caused by an eclipse of the star by the disk). These observations confirmed earlier hints that GRO J1655-40 might be an eclipsing binary: Bailyn et al. (1995a) observed a single eclipse-like event in the photometry on the night of August 17, 1994, and the model of the kinematics of the radio jets proposed by Hjellming & Rupen (1995) gives an inclination of $i = 85$ deg. In spite of the observations of optical eclipses, there has not yet been an unambiguous observation of an X-ray eclipse (e.g. Harmon et al. 1995a). The lack of X-ray eclipses and the presence of optical eclipses puts a tight constraint on the inclination of the orbit.

Unlike most “X-ray novae,” GRO J1655-40 continued to have major outburst events in hard X-rays long after its initial high-energy outburst (see Harmon et al. 1995a). There was an outburst event late March, 1995 (Wilson et al. 1995) and another one starting late July, 1995 (Harmon et al. 1995b). Not surprisingly, the V magnitude of the source during 1995 was typically around $V \approx 16.5$ (e.g. Bailyn et al. 1995b), somewhat higher than the quiescent value of $V \approx 17.3$ (Bailyn et al. 1995a). Furthermore, the shapes of the

light curves from 1995 are complicated. There are night-to-night brightness variations, and the phases of some of the optical minima are not aligned precisely with the spectroscopic phase (Bailyn et al. 1995b). X-ray heating and hot spots on an asymmetric accretion disk probably play a large role in explaining the complex light curves.

After the July/August, 1995 hard X-ray outburst, the source finally settled into true X-ray quiescence. From the period of late August, 1995 to late April, 1996, the source was not detected by BATSE (Robinson et al. 1996). The ASCA X-ray satellite made several pointed observations in late March, 1996 as part of a large multi-wavelength observing program (Robinson et al. 1996). The soft X-ray luminosity was found to be quite low, with $L_x \approx 2 \times 10^{32}$ ergs s^{-1} (assuming a distance of $d = 3.2$ kpc—see Robinson et al. 1996), which is about a factor of 900 times *smaller* than the optical luminosity of the secondary star ($L_2 \approx 47 L_{\odot}$, see Section 6). The extended period of X-ray quiescence ended late April, 1996 when the all sky monitor on the *Rossi X-ray Timing Explorer* satellite detected a sharp increase in brightness in the soft X-rays (Remillard et al. 1996a). The source also brightened significantly in the optical and UV (Horne et al. 1996), and in the radio wavelengths (Hunstead & Campbell-Wilson 1996; Hjellming & Rupen 1996).

We have obtained additional photometry and spectroscopy of GRO J1655-40 February and March, 1996. Much of the March data was taken as part of the larger multi-wavelength program (Robinson et al. 1996). These data show that the mean V magnitude is consistent with its pre-outburst value and that in the optical the system is dominated by light from the secondary star. Since the accretion disk contributes a small fraction of the light and since GRO J1655-40 eclipses, we have a unique opportunity to model the light curves and obtain a reliable measure of the orbital inclination, thereby leading for the first time a reliable mass for a black hole. In Section 2 we describe our quiescent photometric observations. We present an improved spectroscopic ephemeris in Section 3. In Section 4 we discuss the spectral classification of the secondary star. In Section 5 we describe models of the light curves. Section 6 is the discussion section detailing the evolutionary status of the secondary star, the inclination of the radio jet, and the stability of the accretion. A short summary of the paper is presented in Section 7. We have also included an Appendix to this paper which gives a detailed description of the

TABLE 1
JOURNAL OF SPECTROSCOPIC OBSERVATIONS

	1995 April 30-May 4 ^{a,b}	1996 February 24-25 ^c
Telescope	CTIO 4.0 m	CTIO 1.5 m
Detector	Loral 3072 × 1024	Loral 1200 × 800
Grating	KPGL #3 (527ℓ/mm)	KPGL #3 (527ℓ/mm)
Resolution	3.3 Å (FWHM)	4.0 Å (FWHM)
Wavelength Coverage	3850-7149 Å	4673-6657 Å
Number of Spectra	73	12

^aPreviously published in Bailyn et al. 1995b.

^bThe heliocentric Julian date (HJD) range: 2 449 837.580 to 2 449 841.915

^cHJD range: 2 450 137.792 to 2 450 138.890

code used to model the light curves.

2. Observations and Reductions

The spectroscopic observations from April and May, 1995 published in Bailyn et al. (1995b) are summarized in Table 1. Additional spectra were taken in photometric conditions February 24-25, 1996 with the RC spectrograph on the CTIO 1.5 meter telescope. The KPGL #3 grating and the Loral 1200 × 800 CCD combination gave a dispersion of 1.68 Å per pixel. A He-Ar lamp was observed repeatedly to give the wavelength calibrations. In addition to the 12 spectra of GRO J1655-40, we also obtained the spectra of 45 different stars (most with two or more observations), including several radial velocity standards, flux standards, and MK spectral type standards (Morgan & Kennan 1973).

Photometry of the source was obtained February, March, and April, 1996 with the CTIO 0.9 meter telescope and Tek 2048 × 2046 #3 CCD (see Table 2). All of the nights in February, 1996 were photometric and about half of the nights in the March-April, 1996 run were photometric. Standard IRAF tasks were used to process the images to remove the electronic bias and to perform flatfielding corrections. The programs DAOPHOT IIe and DAOMASTER (Stetson 1987; Stetson, Davis, & Crabtree 1991; Stetson 1992a,b) were used to compute the photometric time series of GRO J1655-40 and several field com-

parison stars. The errors in the instrumental magnitudes were estimated by computing the standard deviations in the light curves of several stable field stars. The sizes of these errors were found to be in reasonable agreement with the errors reported by the DAOMASTER program. We have adopted the errors given by DAOMASTER in the analysis presented below. The instrumental magnitudes were transformed to the standard system using previously calibrated field stars (Bailyn et al. 1995a). All of the February, 1996 frames were usable. Out of the all the frames taken in March and April, one frame in *B*, two frames in *R*, and one frame in *I* were not used in any of the analysis because of cosmic ray hits on or very near the image of GRO J1655-40.

3. A Refined Spectroscopic Ephemeris

The 73 spectra from April 30-May 4, 1995 were rebinned to match the slightly larger dispersion and smaller wavelength coverage of the 12 spectra from 1996. The radial velocities of the 85 spectra were found by computing the cross-correlations (Tonry & Davis 1979) against a spectrum of 40 Leo (=HD 89449), a radial velocity standard star of spectral type F6IV (radial velocity = $+6.5 \pm 0.5$ km s⁻¹) that was observed February, 1996. The cross-correlations were computed over the wavelength region between H β and H α , excluding the strong interstellar absorption lines (see Bailyn et al. 1995a) and regions corrupted by bad

TABLE 2
JOURNAL OF PHOTOMETRIC OBSERVATIONS

UT Date	Telescope	Filter	Detector	Number of exposures
1996 February 5,7-20 ^a	CTIO 0.9 m	V	Tek 2k #3	24
1996 February 5,7-20	CTIO 0.9 m	I	Tek 2k #3	23
1996 March 21-31 ^b	CTIO 0.9 m	B	Tek 2k #3	24
1996 March 21-31	CTIO 0.9 m	V	Tek 2k #3	157
1996 March 21-31	CTIO 0.9 m	R	Tek 2k #3	24
1996 March 21-31	CTIO 0.9 m	I	Tek 2k #3	150
1996 April 1 ^c	CTIO 0.9 m	B	Tek 2k #3	2
1996 April 1	CTIO 0.9 m	V	Tek 2k #3	12
1996 April 1	CTIO 0.9 m	R	Tek 2k #3	2
1996 April 1	CTIO 0.9 m	I	Tek 2k #3	9

^aHJD range: 2 450 118.836 – 2 450 133.892

^bHJD range: 2 450 163.711 – 2 450 173.895

^cHJD range: 2 450 174.727 – 2 450 174.895

pixels on the CCDs. Out of the 85 spectra, 84 yielded significant cross correlations (r values greater than 4; see Tonry & Davis 1979). The remaining spectrum had a huge cosmic ray hit and was not used in any of the analysis presented below. A sinusoid fit, excluding the May 2, 1995 data (when the star was partially eclipsed by the disk) was performed giving the spectroscopic elements listed in Table 3. The folded radial velocities and the best fitting sinusoid are shown in Figure 1.

We relaxed the assumption of a circular orbit and attempted to fit the radial velocities to an eccentric orbit. We applied the Lucy & Sweeney test (1971) to check the significance of the derived eccentricity ($e = 0.057 \pm 0.020$). The significance of the eccentric orbit fit is much lower than 5%, indicating the eccentric orbit fit is no improvement over the circular orbit fit to the radial velocities.

The light curves from February and March, 1996 folded on the spectroscopic ephemeris are shown in Figure 2. The light curves are dominated by ellipsoidal variations with maxima at the spectroscopic phases 0.0 and 0.5 (the quadrature phases) and min-

ima of unequal depth at the spectroscopic phases 0.25 and 0.75 (the conjunction phases). During March, 1996 we observed three local extrema: a deep minimum on March 22, a maximum on March 24, and a shallow minimum on March 26. We fit a parabola to the V data from each of these three nights and determined the times of the local extrema from the fits. The times are (HJD 2,450,160+) 4.835 ± 0.010 , 6.806 ± 0.010 , and 8.766 ± 0.010 . The spectroscopic phases of these three times are 0.261 ± 0.008 , 0.013 ± 0.008 , and 0.760 ± 0.008 , very close to their expected values of 0.25, 0.00, and 0.75. Thus, the phasing of the March, 1996 V light curve is consistent with the spectroscopic ephemeris given in Table 3.

Our revised spectroscopic period can be compared with the period of $2^d 2616 \pm 0^d 0016$ found by van der Hooft et al. (1996) based on photometry from May to July, 1995. Our period agrees with theirs to within their errors. However van der Hooft et al. (1996) then used spectroscopic fiducial points (including the one in Bailyn et al. 1995b) and derived the following

TABLE 3
ORBITAL PARAMETERS FOR GRO J1655-40

parameter	result
Orbital period, spectroscopic (days)	2.62157 ± 0.00015
K velocity (km s^{-1})	228.2 ± 2.2
γ velocity (km s^{-1})	-142.4 ± 1.6
T_0 (spectroscopic) (HJD 2 440 000+)	$9\,839.0763 \pm 0.0055$
Mass function (M_{\odot})	3.24 ± 0.09

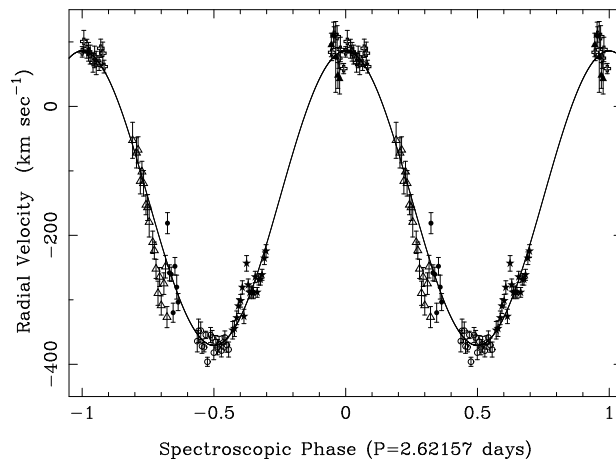


Fig. 1.— The folded radial velocities of GRO J1655-40 and the best fitting sinusoid (see Table 3). Each point has been plotted twice. Open diamonds indicate data from April 30, 1995; open triangles, filled stars, and open crosses indicate data from May 2, 3, and 4, 1995, respectively. The velocities from February 24, 1996 are indicated by the filled triangles, and the filled circles indicate data from February 25, 1996. Parts of this figure appeared in Bailyn et al. (1995b).

ephemeris:

$$T_{\min}(\text{HJD}) = 2\,449\,838.4279(30) + 2.62032(50)N \quad (1)$$

This period differs from our period by 2.5σ . Also, the phases of the three local extrema in our V light curve from March 1996 are by the above ephemeris 0.568 ± 0.024 , 0.320 ± 0.024 , and 0.068 ± 0.024 , significantly different from their expected values of 0.50, 0.25, and 0.00. Bailyn et al. (1995b) reported great difficulties in phasing up their light curves from March and April, 1995—no single period could align all of the optical minima with the radial velocities. It appears that the light curves from May to July, 1995 still suffer from phasing problems, although to a much smaller extent than the earlier light curves from 1995. The period

derived solely from the radial velocities appears to be the most reliable.

The refined period of $P = 2^{\text{d}}62157 \pm 0^{\text{d}}00015$ represents a great improvement in accuracy over the previous value given in Bailyn et al. (1995b). Using this new period, we can now compute accurately the orbital phase of observations made in 1994 and late 1995. For example, Bailyn et al. (1995a) presented photometry from August 17, 1994 which showed evidence for an eclipse (the source got fainter and redder then bluer and brighter over the 4.5 hours of observations). Only one such eclipse-like event was observed in 1994. Using the refined orbital period, we find that the spectroscopic phase of the time of minimum

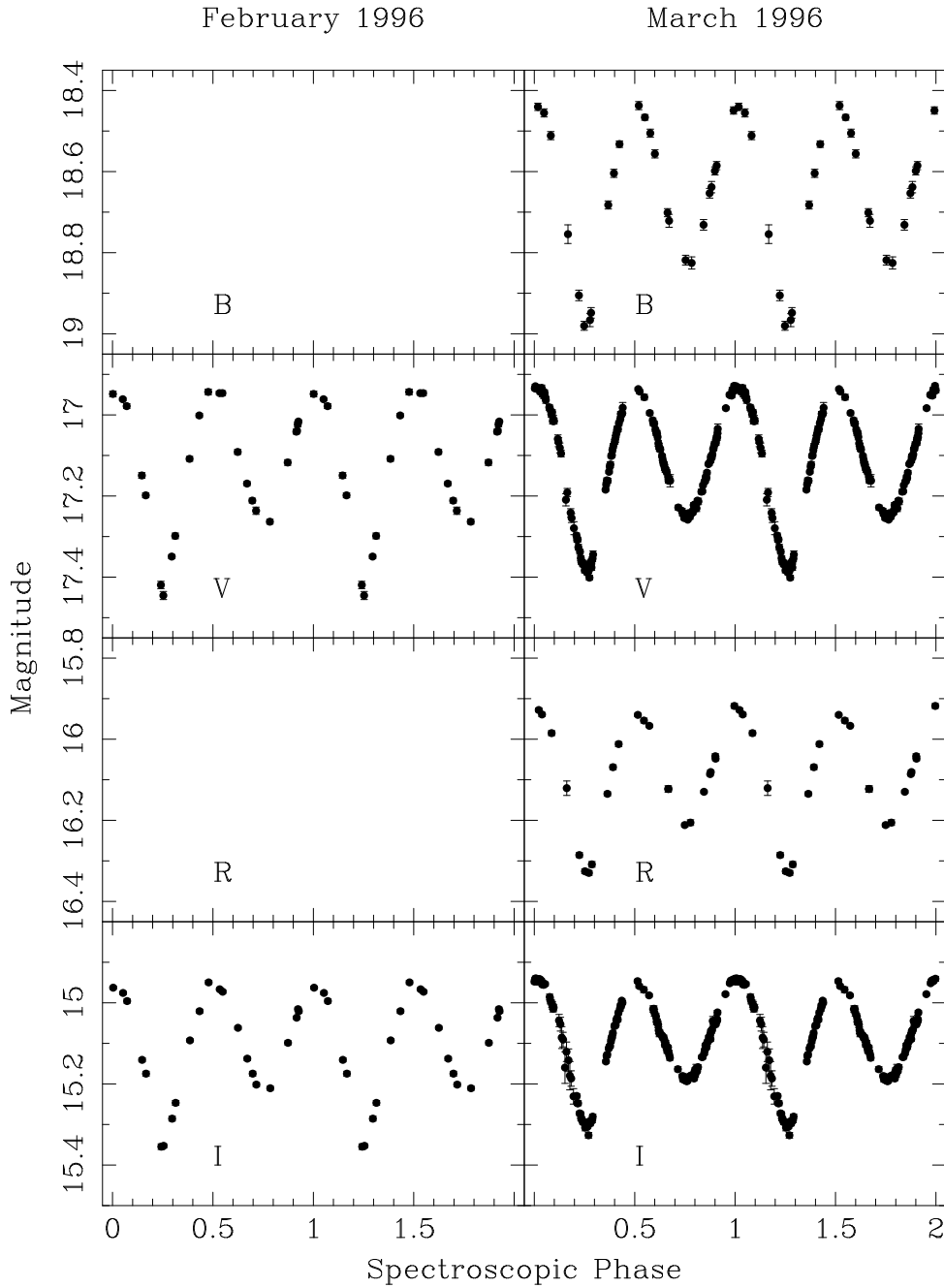


Fig. 2.— The light curves from February, 1996 (left panels) and March, 1996 (right panels) folded on the spectroscopic ephemeris (Table 3) are shown. Each point has been plotted for clarity. Error bars are shown for all of the points, but in many cases the size of the errors is smaller than the symbols.

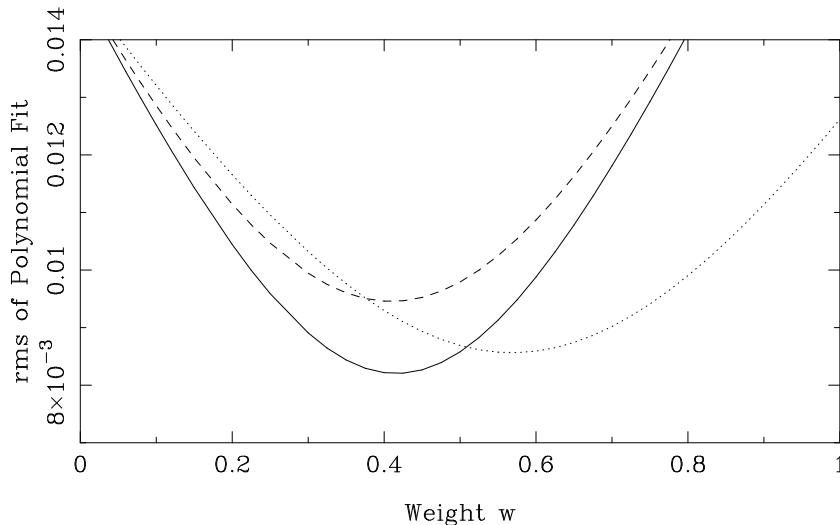


Fig. 3.— The rms residuals of a polynomial fit to the difference spectrum as a function of the weight w for three different template stars: an F3IV star (solid line), an F3V star (dotted line), and a G0V star (dashed line). In each case, the minimum of the curve can be accurately computed. The restframe spectrum was from 1996. See the text for more details.

light (estimated to be at the heliocentric Julian date 2,449,581.63) is 0.80. Curiously enough, the sharp optical minimum observed April 2, 1995 (see Bailyn et al. 1995b) also has a spectroscopic phase of 0.80 (the phasing offsets of the light curves will be discussed more below). The ASCA X-ray satellite observed GRO J1655-40 at the end of August 23, 1994 (Inoue et al. 1994). During most of this observation the X-ray flux stayed relatively low. Also, the X-ray spectrum from August 23 was quite different when compared to subsequent observations, leading to the speculation that an X-ray eclipse was observed (Inoue 1995, private communication). It turns out that the spectroscopic phases of the August 23 ASCA observations are from 0.27 to 0.36—i.e. the star was *behind* the compact object. Thus some other mechanism must be invoked to explain the X-ray light curve and spectrum from August 23, 1994.

4. Spectral Classification

During the April-May, 1995 observing run, the spectra of 33 different stars of spectral type F through K and luminosity classes V through III were taken. During the February, 1996 run, we obtained the

spectra of 45 different stars, including nine Morgan-Keenan (1973) spectral type standard stars of class F. We used the technique outlined in Orosz et al. (1996) to classify the 1995 and 1996 spectra of GRO J1655-40. First, each continuum-normalized spectrum of GRO J1655-40 is shifted to zero velocity and the lot of them are averaged together, creating a “restframe” spectrum. To help minimize the effects of an occasional cosmic ray, a “min-max” rejection scheme was used where the lowest and highest values at each pixel were rejected before the average was computed. Then, the velocity shifts between the comparison spectra and the restframe spectrum are removed. Finally, the steps involved in the comparison are (1) each continuum-normalized and shifted comparison spectrum is scaled by a factor w (where $0 \leq w \leq 1$) and subtracted from the normalized restframe spectrum, (2) a low order polynomial is fit to the difference spectrum, (3) the rms residuals of the fit (computed over the same region used to compute the cross-correlations) is recorded, and (4) steps (1) through (3) are repeated using different scaling factors until the minimum rms is found, corresponding to the “smoothest” difference spectrum. In finding

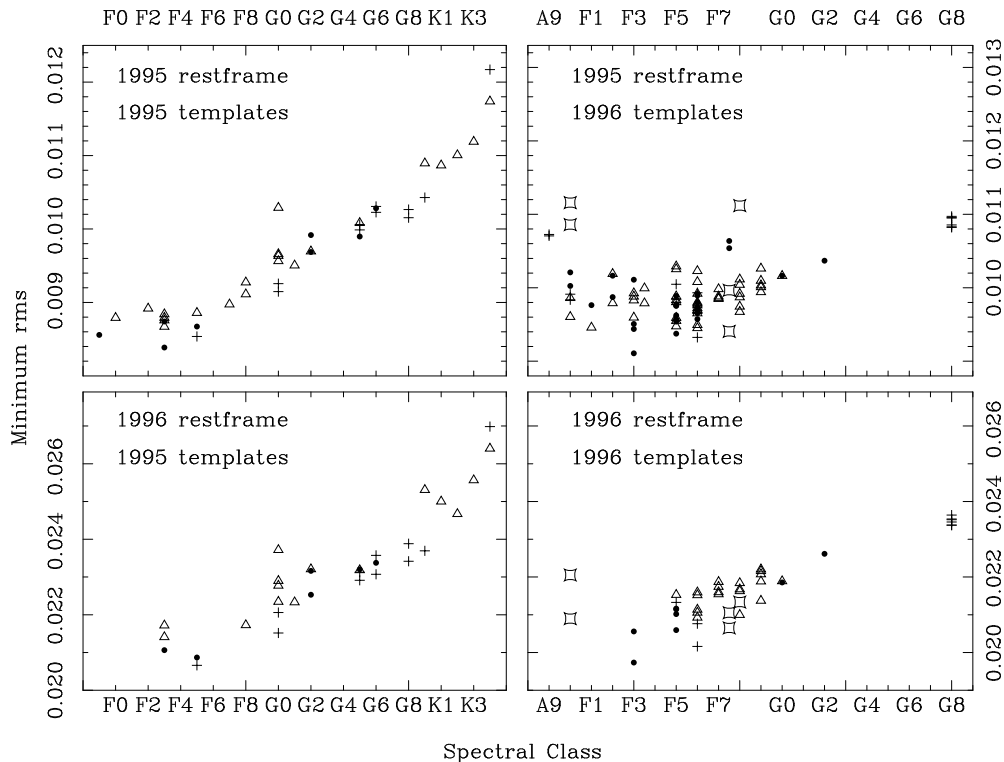


Fig. 4.— The minimum rms (see the text) is plotted as a function of the spectral type of the template for the four different groups. The plotting symbol indicates the luminosity class of the template: open triangles for dwarfs, filled circles for subgiants, crosses for giants, and curved squares for supergiants. Templates that had a weight $w > 1$ are not shown (see the text). In each case, the lowest *overall* rms values occur for the spectral classes F3 to F5. Note that many of the template stars had two or more observations, so that the total number of template stars used is less than the number of symbols shown.

the rms of the fits to the difference spectra, we were careful to avoid interstellar absorption lines and regions corrupted by bad columns on the CCDs. Figure 3 shows a plot of the rms of the fit to the difference spectrum as a function of the weight w for some representative cases. In each case, the minimum of the curve can be determined accurately. All of the above four steps are done on all of the comparison spectra, and the comparison spectrum that has the lowest overall rms value is taken to be the spectrum whose absorption lines most closely match those in the restframe spectrum. The relative fluxes of the restframe spectrum and the difference spectrum give an estimate of the fraction of the total light due to the accretion disk.

We have two restframe spectra of GRO J1655-40, one each from 1995 and 1996 (for the 1995 restframe spectrum, we did not include the spectra from May 2, 1995 because the star was partially eclipsed by the disk). We also have two sets of template comparison spectra from the same times. Every spectrum in each set of templates was compared against both rest-

frame spectra. Since the 1995 spectra have a slightly higher spectral resolution than the 1996 spectra and since the 1996 restframe spectrum has a lower signal-to-noise ratio than the 1995 restframe spectrum, a given template spectrum will have a slightly higher minimum rms value when compared against the 1996 restframe spectrum. We therefore grouped the comparisons into four different cases: the 1995 template spectra compared against the 1995 restframe spectrum, the 1995 template spectra compared against the 1996 restframe spectrum, etc. The relative values of the minimum rms within each group can be used to judge the best spectral match to the given restframe spectrum. Figure 4 shows the minimum rms value plotted against the spectral type of the template spectrum for the four different cases. In all four cases, there is a clear trend: the best matches for the GRO J1655-40 restframe spectra are the F3-F5 stars. Stars with spectral types later than F6 or earlier than F3 provide much poorer matches to the restframe spectra. Based on the values of the weight w found for the best matches, we conclude that the accretion disk

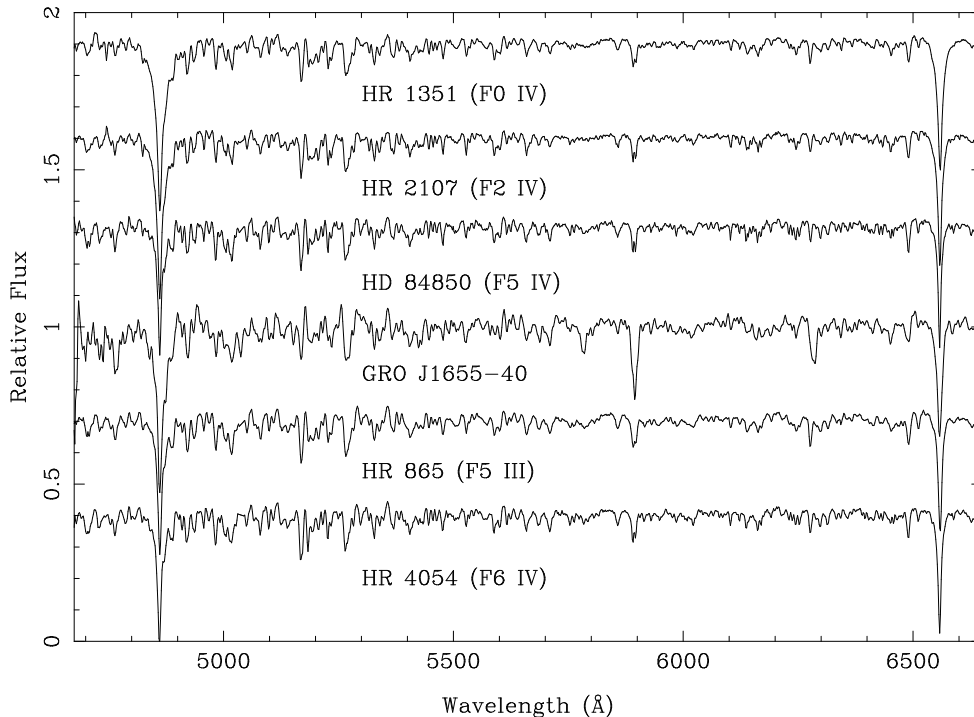


Fig. 5.— The restframe spectrum of GRO J1655-40 from February, 1996 (fourth from the top) and the spectra of several F subgiants and giants. The anomalous strengths of the absorption lines near 5900 Å and 6300 Å in the spectrum of GRO J1655-40 are due to interstellar absorption. Each spectrum has been normalized to its continuum fit, and offsets have been applied for clarity.

contributed about 50% of the flux in V during April and May, 1995, and less than 10% of the flux in V during February, 1996.

This comparison technique is relatively sensitive to the temperature class of the comparison star and relatively insensitive to the luminosity class of the comparison star. We therefore cannot reliably determine the luminosity class of the secondary star from this technique alone. However, in the case of GRO J1655-40, a main sequence F star is much too small to fill the Roche lobe (Bailyn et al. 1995b), so the secondary star must be somewhat evolved. Also, in the case of the 1996 restframe spectrum, many of the early F dwarf template stars were excluded because a weight of $w > 1$ was required to get the minimum value of the rms. Hence, we are left with mainly subgiants and giants. So, based on these other pieces of evidence, we conclude the secondary star in GRO J1655-40 is a subgiant, giving its full spectral classification as F3-F5 IV. Indeed, with the exception of the strong interstellar features, it is difficult to tell the difference between the 1996 restframe spectrum of GRO J1655-40 and the spectra of the nearby F subgiants and giants (see Figure 5).

The 1995 spectra of GRO J1655-40 were examined in more detail to see if the best fitting spectral type depends on the orbital phase. There was no indication of any change in the spectral type as a function of phase. Further details can be found in Orosz (1996).

5. Light Curve Models

The light curves shown in Figure 2 appear to be almost completely ellipsoidal—there are two equal maxima per orbit and two minima of unequal depth per orbit. The minimum at the spectroscopic phase 0.25 (when the star is behind the compact object) is deeper because the gravity darkening near the L_1 point is greater and hence the star appears darker (see Avni 1978 and the Appendix). The symmetry and smoothness of the GRO J1655-40 light curves from 1996 are in strong contrast to the light curves for the other black hole binaries (e.g. McClintock & Remillard 1986; Wagner et al. 1992; Chevalier & Ilovaisky 1993; Haswell et al. 1993; Haswell 1996; Remillard et al. 1996b; Orosz et al. 1996), where the light curves are complicated by “flickering” about the mean light curve and by large asymmetries in the light curve that slowly change with time (e.g. Haswell 1996).

TABLE 4
INPUT MODEL PARAMETERS

parameter	description	comment
i	inclination	free
Q	mass ratio ($M_1/M_2 > 1$)	free
r_d	outer radius of the disk ^a	free
r_{inner}	inner radius of the disk ^a	fixed at 0.005
T_{disk}	disk temperature at the outer edge	free
ξ	power law exponent on disk temperature radial distribution	free
β_{rim}	flaring angle of the disk rim	free
L_x	X-ray luminosity of the compact object	fixed at 0.0
W	X-ray albedo	fixed at 0.5
T_{eff}	polar temperature of the secondary	fixed at 6500 K
β	gravity darkening exponent	fixed at 0.25
$u(\lambda)$	linearized limb darkening parameter	fixed ^b
P	orbital period	fixed at 2 ^d 62157
$f(M)$	mass function	fixed at $3.24 M_{\odot}$
Ω	ratio of rotational angular velocity to orbital angular velocity	fixed at 1.0
f	Roche lobe filling factor	fixed at 1.0

^aThe disk radii are scaled to the effective Roche lobe radius of the compact object.

^bLimb darkening parameters from Al-Namity (1978) and Wade & Rucinski (1985).

Because the light curves from February and March, 1996 are smooth and symmetric and because the luminosity of the star dominates (i.e. the fraction of the light from the disk is small, see Section 4), we have a unique opportunity to model the light curves and obtain a reliable constraint on the orbital inclination. We have developed a detailed code based on the work of Avni (Avni & Bahcall 1975; Avni 1978) to model the light curves, which is fully described in the Appendix. The code uses full Roche geometry to account for the distorted secondary, and light from a circular accretion disk is included. The code also handles mutual eclipses by the star and the disk. The effects of X-ray heating on the secondary star are included as well. There are several input model parameters which are summarized in Table 4. See the Appendix for detailed discussions of these parameters and their

meaning.

For simplicity, we have fixed several of the input parameters at reasonable values. For example, we know the spectral type of the star (see the previous section), from which we can get its effective temperature. The effective temperature of 6500 K is appropriate for an F5 IV star (Straižys & Kuriliene 1981) and we will adopt the effective temperature of 6500 K as the polar temperature. The gravity darkening exponent is fixed at 0.25 since the star has a radiative envelope (see the Appendix). The limb darkening coefficient $u(\lambda)$ is better determined from model atmosphere computations, and we used values interpolated from tables given by Wade & Rucinski (1985). For fits to the 1996 light curves, we have fixed the X-ray luminosity at 0, based on the ASCA observation in early 1996 that found $L_x \approx 2 \times 10^{32}$ ergs s⁻¹,

TABLE 5
 FITS TO THE MARCH, 1996 PHOTOMETRY

parameter	model 1	model 2 ^a	model 3
i (degrees)	69.50 ± 0.08	74.7 ± 1.2	69.54 ± 0.08
Q	2.99 ± 0.08	3.3 ± 0.5	3.50 ± 0.08
r_d	0.747 ± 0.010	0.71 ± 0.01	0.748 ± 0.011
T_{disk} (K)	4317 ± 75	4525 ± 102	4429 ± 75
β_{rim} (degrees)	2.23 ± 0.18	1.54 ± 0.4	2.91 ± 0.18
ξ	-0.12 ± 0.01	-0.22 ± 0.01	-0.13 ± 0.01
L_x	0.0 (fixed)	0.0 (fixed)	0.0 (fixed)
W	0.5 (fixed)	0.5 (fixed)	0.5 (fixed)
T_{eff} (K)	6500 (fixed)	6500 (fixed)	7000 (fixed)
χ^2_{ν}	1.1551	3.2391	1.1816

^aNo checking for eclipses done.

almost three orders of magnitude lower than the optical luminosity of the secondary star ($L_2 \approx 47 L_{\odot}$, see the next Section). In the case where $L_x = 0$, the exact value of the X-ray albedo W is of course irrelevant. For fits to the March 1995 light curves where $L_x \gg L_2$, we have adopted $W = 0.5$ (see the Appendix), although other values of the X-ray albedo W have been used (for example van der Hooft et al. (1996) used $W = 0.4$). Since there is mass transfer taking place, we assume the star fully fills its Roche lobe and that it is in synchronous rotation.

For fits to the 1996 light curves, we are left with six free parameters. The six free parameters in the model are the inclination of the orbit (i), the mass ratio ($Q \equiv M_1/M_2$), the outer radius of the disk in terms of the primary’s effective Roche lobe radius (r_d), the temperature at the outer edge of the disk (T_{disk}), the flaring angle of the rim of the disk (β_{rim} , where the thickness of the disk at the outer edge is given by $2r_d \tan \beta_{\text{rim}}$), and the power law exponent on the disk’s radial temperature distribution (ξ , where the disk temperature varies with radius as $T(r) = T_{\text{disk}}(r/r_d)^{\xi}$).

We first fit models to the *BVRI* light curves from March, 1996, as the phase coverage and spectral coverage from that time is the most complete. We folded the data on the photometric phase convention used in the code where the photometric phase 0.0 corresponds

to the time the secondary is directly in front of the compact object (i.e. $T_0(\text{photo}) = T_0(\text{spect}) + 0.75P$). As discussed in Section 3, the phases of the three local extrema observed in March, 1996 are all late in phase by ≈ 0.011 . We found that the model fits were slightly better after a phase shift of 0.011 was removed from the folded curves. Since there are far fewer points in the *B* and *R* filters, we gave each point in *B* and *R* seven times more weight when computing the chi-square of the fit. This procedure resulted in equal weight being given to each filter. Figure 6 shows the fits and the residuals and Table 5 lists the model parameters (under “model 1”). Note that the data in all four filters were fit simultaneously. The model fits the observed light curves from all four filters quite well—the scatter in the residuals is typically less than 0.02 magnitudes. The 1σ statistical errors for each parameter were estimated using primarily a Monte Carlo “bootstrap” method (Press et al. 1992—see the Appendix). For this model, the accretion disk contributes about 5% of the flux at 5500 Å, consistent with the measurement of $\leq 10\%$ from late February, 1996 (see the previous Section).

As a test of the accuracy of the 1σ errors derived from the bootstrap analysis, we performed fits to the March 1996 light curves with the value of Q at fixed at several different input values. The other five parameters were free and adjusted to find the minimum

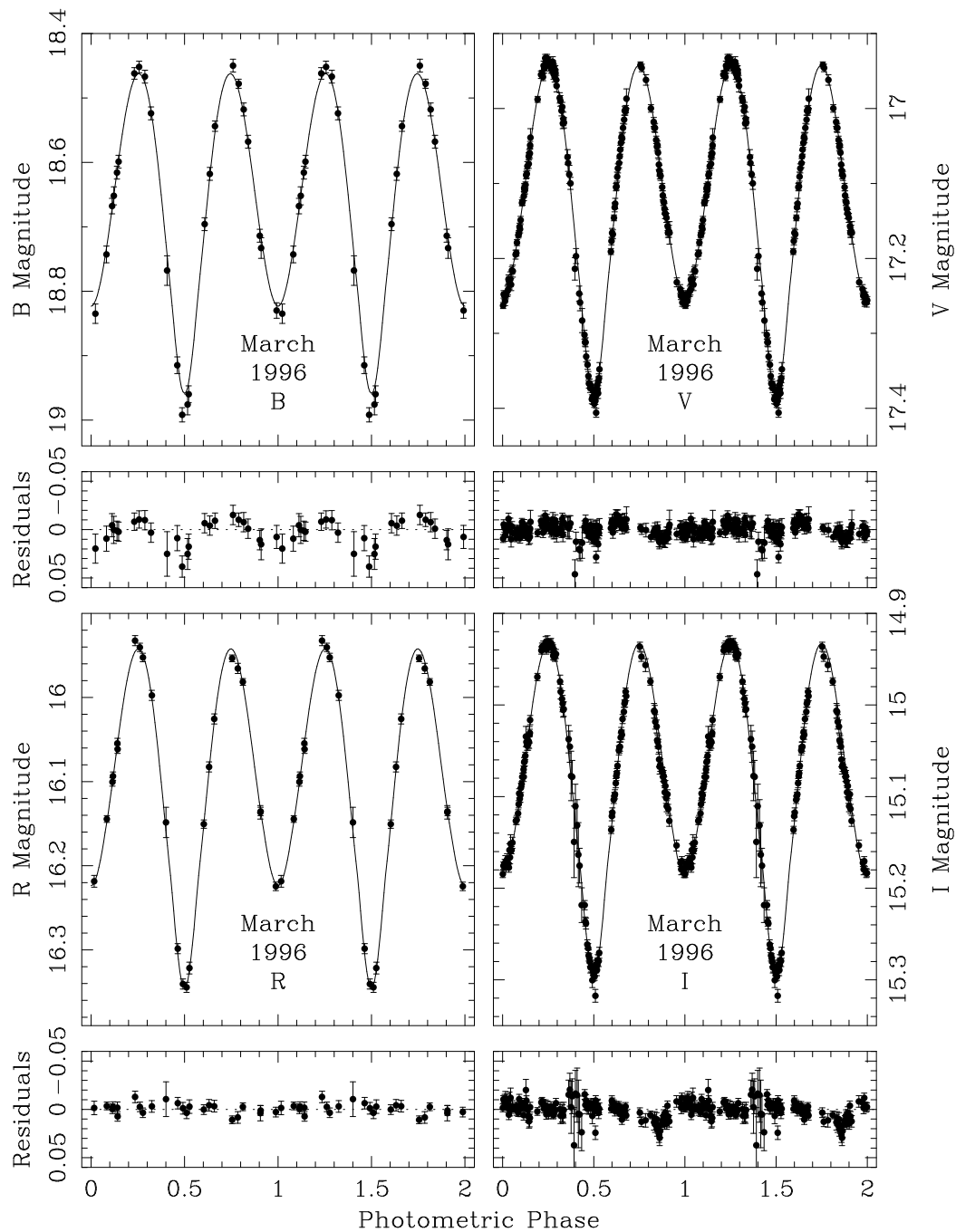


Fig. 6.— The model fits to the B , V , R , and I light curves from March, 1996 (large panels) and the residuals of the fits (i.e. the data $minus$ the model—small panels). Table 5 gives the model parameters under “model 1.”

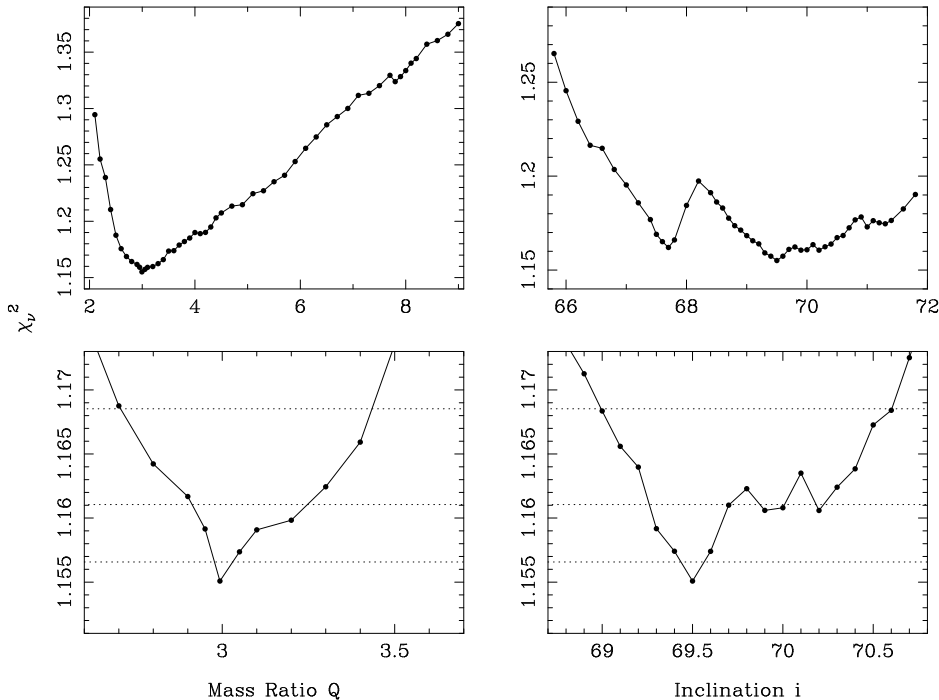


Fig. 7.— Upper left: The value of the reduced chi-square as a function of the mass ratio Q , where the value of Q is fixed at each input value and the other five parameters are adjusted until the chi-square is minimized. Lower left: An expanded view of the χ^2_ν vs. Q curve. The dotted lines indicate the change in the chi-square required for a 1, 2, and 3σ change in a single parameter (i.e. $\Delta\chi^2 = 1, 4,$ and 9). Upper and lower right: similar to the left panels, but for fits with the inclination angle i fixed at various input values.

reduced chi-square at each input value of Q . The left panels of Figure 7 shows the χ^2_ν vs. Q curve. The dashed lines shown in the lower left panel of Figure 7 indicate the change in χ^2_ν representing a 1, 2, and 3σ change in a single parameter (i.e. $\Delta\chi^2 = 1, 3,$ and 9). A change in Q of 0.08 (the 1σ error derived from a Monte Carlo bootstrap analysis) in either direction from its value at the minimum causes the χ^2_ν to increase by approximately the amount indicated by the lowest dashed line. The right panels of Figure 7 show the equivalent computation done with the value of i fixed at several different values. Like before, a 1σ change in the parameter i (0.08) from the best value causes the value of χ^2_ν to increase by approximately the amount indicated the lowest dashed line in the lower right panel. The χ^2_ν v.s. i curve has a secondary minimum at $i = 67.7$ deg and $\chi^2_\nu = 1.1620$, which is greater than the 2σ deviation from the primary minimum at $i = 69.5$ deg and $\chi^2_\nu = 1.1551$. While we are confident that the errors derived from the bootstrap analysis are a reasonable representation of the true internal statistical errors, there may be systematic errors due to physical effects not included in the model. Given how well the model fits the data, we

suspect that such systematic errors are likely to be small. We are also confident that we have found the global minimum of χ^2_ν since we have searched a large amount of parameter space.

For each model with Q fixed at a given input value, there exists a value of the inclination i found from the best fit. For the whole range of Q shown in the upper left panel of Figure 7, the corresponding best values of i range from $68.40 \leq i \leq 71.1$ deg. Likewise, for the models with the inclination angle i fixed at several values (the upper right panel of Figure 7), the corresponding best values of the mass ratio Q are in the range $2.52 \leq Q \leq 4.23$. Thus, the key geometrical parameters i and Q vary little and seem to be reasonably well determined. Based on the behavior of χ^2 near the minimum, we adopt the 1σ and 3σ ranges of the inclination i :

$$69.42 \text{ deg} \leq i \leq 69.58 \text{ deg} \quad (1\sigma)$$

$$69.0 \text{ deg} \leq i \leq 70.6 \text{ deg} \quad (3\sigma)$$

and the mass ratio Q :

$$2.91 \leq Q \leq 3.07 \quad (1\sigma)$$

$$2.60 \leq Q \leq 3.45 \quad (3\sigma).$$

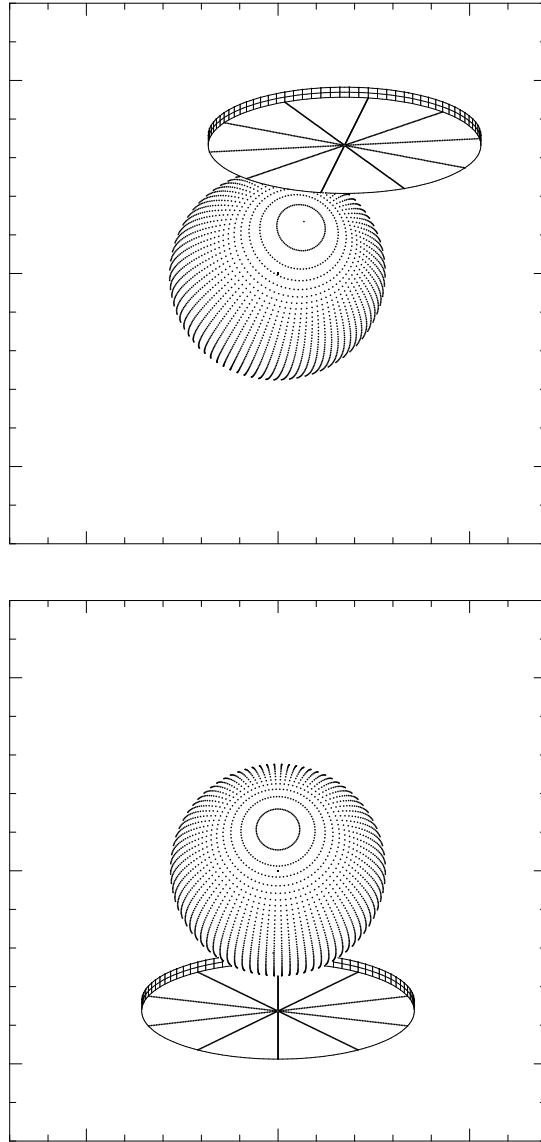


Fig. 8.— The system as it appears projected onto the plane of the sky for the model parameters given in Table 5, model 1. The photometric phase is 0 deg for the bottom panel and 170 deg for the top panel.

The geometry of the system is shown schematically for two different phases in Figure 8. Note that the compact object is *not* eclipsed by the secondary star. We would therefore *not* expect to see X-ray eclipses (assuming the X-rays are emitted from a relatively small region centered on the compact object), and in fact no X-ray eclipses have been seen (e.g. Harmon et al. 1995a). The star does block part of the disk (and vice-versa) at certain phases, so we expect to still see grazing optical eclipses, the depths of which depend on the size of the disk and the relative brightnesses of each component. In order to assess how important the grazing eclipses are in determining the final overall shapes of the light curves, we performed a model fit to the *BVRI* data from March, 1996 where the eclipse checking routines were turned off. In this case the model light curve is just the normal ellipsoidal light curve from a Roche lobe filling star plus a constant flux from the accretion disk (where the amount of disk light relative to the amount of star light in general depends on the filter bandpass). Table 5 gives the values of the parameters (under “model 2”). The fit is poor, as one can deduce from the relatively large value of the reduced chi-square ($\chi^2_\nu = 3.239$, compared to $\chi^2_\nu = 1.1551$ for model 1). The fits are poor when eclipses are not accounted for in the computations for two reasons: (i) the difference in the depths of the two minima in the model light curve are too small, and (ii) the dependence of the light curve amplitude with color is not properly accounted for by the model (the amplitude of the observed light curve is largest in *B* and smallest in *I*, see Figure 2).

Our numerical experiments also show that the final fitted parameters do not depend strongly on the assumed secondary star parameters. For example, in the case of a Roche lobe-filling star, the temperature will not be constant over the surface (see Equation (A3) of the Appendix). In particular, the side of the star near the L_1 point should be the coolest. The temperature of 6500 K corresponding to the observed spectral type therefore represents some kind of flux-weighted average of the temperatures over the surface, and technically not the star’s polar temperature. However, our spectral coverage was not uniform in phase and spectra used to determine the spectral type mainly came from phases near the quadrature phases. The temperatures corresponding to the brightest parts of the projected stellar disk at these phases are within ≈ 200 K of the polar temperature. Also, we could not detect any change in the spectral

type of the individual observations as a function of phase (this includes the data from May 2, 1995 when the star was behind the disk and the L_1 point was in full view—see Orosz (1996)), which suggests other factors are at work when the observed spectrum at a given phase is produced. Thus, we believe we are not making a large error when adopting the temperature derived from the observed spectral type as the polar temperature. In this same vein, we fit a model to the March, 1996 data where the polar temperature of the secondary star was 7000 K, appropriate for an F2 IV star (Straizys & Kuriliene 1981). The results for the geometrical parameters, given in Table 5 under “model 3”, are quite similar to the results using $T_{\text{eff}} = 6500$ K (model 1). Finally, we compared the linearized limb darkening parameters $u(\lambda)$ interpolated from tables given by Al-Naimiy (1978) and Wade & Rucinski (1985). The shapes of the $u(\lambda)$ curves were very similar—the only large differences occurred for wavelengths blueward of the *B* band. As a result, the fits to the *BVRI* light curves of GRO J1655-40 were similar when the limb darkening coefficients were used from either source.

The stellar evolution models (see the Discussion) indicate the secondary has a radiative envelope. We have therefore adopted a gravity darkening exponent of $\beta = 0.25$. We tried a model fit to the light curves with the gravity darkening exponent set to $\beta = 0.08$, the value appropriate for stars with convective envelopes (Lucy 1967). The model fits were much worse in this case (we could not find a fit with $\chi^2_\nu < 2$). When $\beta = 0.08$, the temperature contrast over the star is smaller (see Equation (A3) of the Appendix), leading directly to a smaller brightness contrast, especially between the side of the star near the L_1 point and the opposite side. Since the brightness contrast between the side facing the compact object and the opposite side is greatly reduced, the inclination needs to be higher to produce the same observed amplitude of the light curves. However, as the inclination grows closer to 90 deg, the eclipses become deeper and the fine balance between the primary and secondary eclipse depths is disturbed, making the *simultaneous* fits to all four colors much more difficult. Thus, based both on the stellar evolution models and the quality of the fits, we conclude that the gravity darkening exponent of $\beta = 0.25$, appropriate for a star with a radiative envelope, is the correct choice.

As one can see from Figure 2, the shapes of the February, 1996 light curves are almost identical to

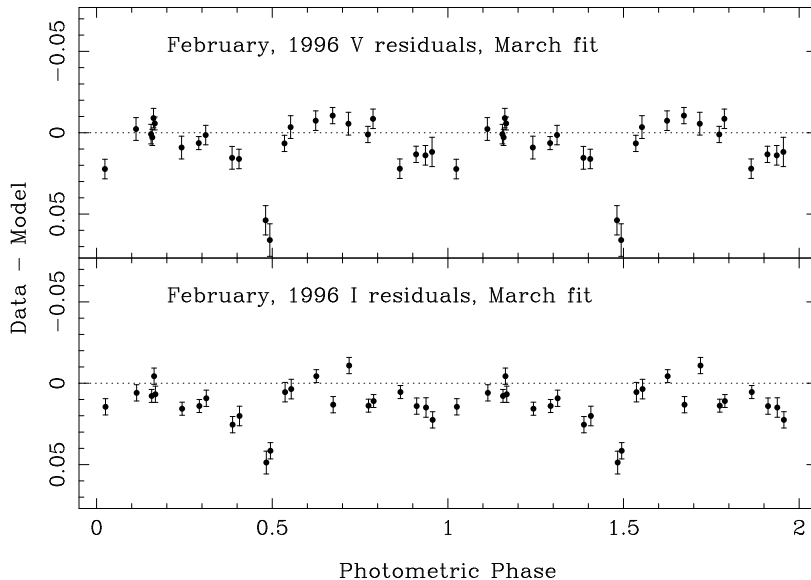


Fig. 9.— The two panels show the February, 1996 data *minus* the March, 1996 model (Table 5, model 1).

the shapes of the light curves from March, 1996. The only noticeable difference between the two curves occurs near the minimum at the photometric phase 0.5 (which is the spectroscopic phase 0.25): that minimum in the February light curves is slightly deeper than that minimum in the March light curves. Not surprisingly, models that fit the March, 1996 data are consistent with the February, 1996 data (Figure 9): the residuals in the *V* band have a mean of 0.009 and a standard deviation of 0.019 and the residuals in the *I* band have a mean of 0.013 and a standard deviation of 0.013. The only deviant points in the two filters are those near the photometric phase 0.5 which are about 0.05 magnitudes *fainter* than the model that fits the data from March.

The light curves of GRO J1655-40 from March and April, 1995 (see Bailyn et al. 1995b) look quite different from the light curves from 1996 (Figure 2). First of all, the source was about 0.7 to 0.8 magnitudes brighter in *V* during early 1995 than it was during early 1996, probably a direct result of the fact that there was still considerable hard X-ray activity taking place during that time (e.g. Wilson et al. 1995). In 1995, the minimum near the spectroscopic phase 0.75 (when the secondary star is in front of the com-

pact object) is the deeper of the two, opposite of the situation in the 1996 light curves. There are large asymmetries in the 1995 light curves, and the phases of the minima of the three light curves shown in Bailyn et al. (1995b) do not all line up properly with the spectroscopic phase (the difference in phase is as large as 0.05). Similar (but smaller) phase shifts in the optical light curve minima have been seen in some low mass X-ray binaries (for example X1822-371, Hellier & Mason 1989). The phase shifts of the minima are presumably caused by large distortions in the accretion disk. Hellier & Mason (1989) invoked a thick accretion disk where the thickness of the rim depended strongly on the azimuth angle to explain the X-ray and optical light curves of X1822-371. It is quite clear that our simple model where the disk is a flattened azimuthally symmetric cylinder will not be able to produce a model light curve whose minima are shifted from their expected phases.

Out of the three light curves from 1995 presented in Bailyn et al. (1995b), the *V* and *I* light curves from March 18-25, 1995 are the most symmetric. In addition, the minima of these light curves line up approximately at their expected phases when the data are folded on the revised spectroscopic ephemeris pre-

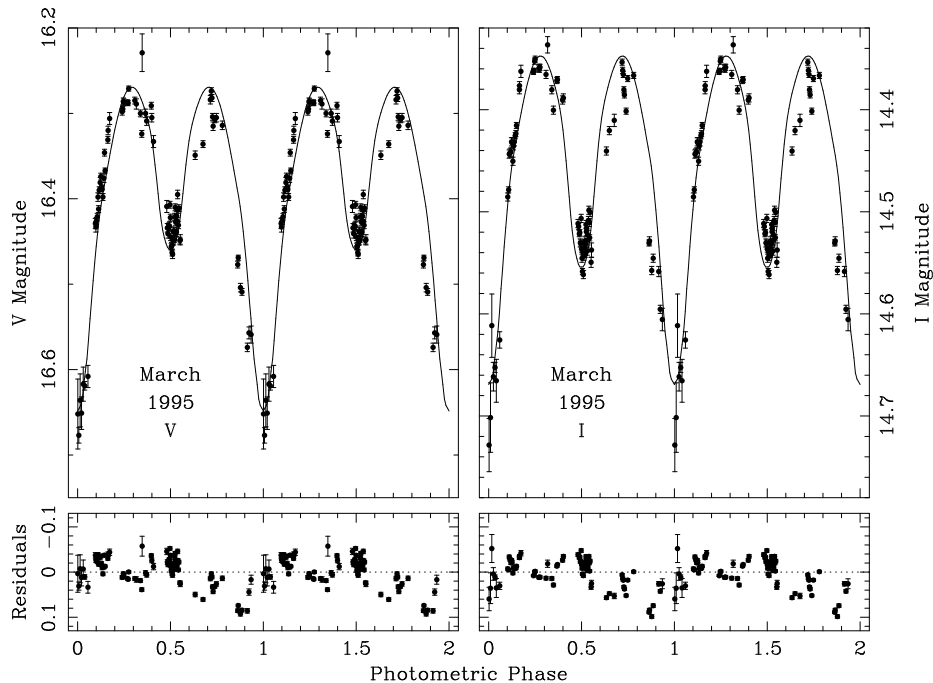


Fig. 10.— The models fits to the V and I light curves from March, 1995 (top panels) and the residuals of the fits (i.e. the data *minus* the model—bottom panels). Table 6 gives the model parameters. Note the scale changes in the plots compared to Figure 6. These data were published previously in Bailyn et al. 1995b.

sented in Table 3 (whereas the minima of the later light curves do not). We attempted, a model fit to the March 18-25, 1995 data to see if the overall shape of those two light curves can be explained by our model (as discussed above we will not be able to model *all* of the 1995 light curves because of the large phase shifts of the minima of the other light curves). For fits to the March, 1995 light curves, we must take into account X-ray heating of the secondary star. The part of the secondary star facing the compact object will be hotter and hence brighter than it would otherwise be in the absence of any external heating. We set the X-ray albedo at $W = 0.5$ and let the X-ray luminosity of the compact object L_x be a free parameter. We fixed the inclination at $i = 69.50$ deg and the mass ratio at $Q = 2.99$, the values found from the model fit to the March, 1996 light curves. The results are listed in Table 6, and Figure 10 shows the fits.

Considering the simplicity of the model, the overall shapes of the V and I light curves are fit reasonably well. There is considerable “flickering” about the mean light curve with deviations larger than the observational errors, resulting in the large value of the

reduced chi-square. Note the difference in the disk parameters between the fits to the March, 1995 and March, 1996 data: the disk is much larger and hotter in 1995. It is interesting to note that the disk and the star contribute roughly equal amounts of flux in the V band for the model that fits the March, 1995 data, which is in good agreement with the value of the disk fraction estimated from the spectra from April and May, 1995 (which were *not* simultaneous with the photometry). The observed X-ray luminosity, as determined from the BATSE daily averages, varied by about a factor of four between March 18 and March 25, 1995, with $5.7 \times 10^{36} \lesssim L_x \lesssim 2.3 \times 10^{37} \text{ erg s}^{-1}$ (S. N. Zhang, private communication). Considering the simplistic way the X-ray heating is handled in the model, the fitted value of $L_x = 3.7 \times 10^{36} \text{ ergs s}^{-1}$ is remarkably close to the observed range. A slightly lower value of the X-ray albedo W (like the value of $W = 0.4$ used by van der Hooft et al. 1996) would require a larger value of L_x to produce the same heating effect (e.g. see Equation (A23) of the Appendix), so we do not consider the slight difference between the observed X-ray luminosity and the fitted luminosity to be a problem. Finally, we note that the depth and

TABLE 6
 FITS TO THE MARCH, 1995 PHOTOMETRY

parameter	March, 1995 model 4
i (degrees)	69.50 (fixed)
Q	2.99 (fixed)
r_d	0.95 ± 0.01
T_{disk} (K)	6694 ± 100
β_{rim} (degrees)	12.6 ± 0.1
ξ	-0.18 ± 0.01
L_x (ergs s $^{-1}$)	3.72×10^{36}
W	0.5 (fixed)
T_{eff} (K)	6500 (fixed)
χ^2_ν	66.0

shape of the minimum at the photometric phase 0.5 is sensitive to the amount of X-ray heating. Given that the observed hard X-ray flux from the source varied by about a factor of four during March 18-25, 1995, we should not be surprised to see a large amount of scatter in the optical light curves around phase 0.5. In summary, although we cannot fit every detail in the March, 1995 light curves, we conclude that the basic overall shapes of the light curves (i.e. the relative depths of the minima) can be explained by the effects of X-ray heating on the secondary star. To explain the phase-shifted minima of the other 1995 light curves, we would probably have to invoke an accretion disk whose shape and brightness profile are grossly distorted—something which is beyond the scope of our current model.

The code also computes radial velocities. For a Roche-lobe filling star, the center of light does not precisely follow the center of mass of the star, resulting in a slightly distorted radial velocity curve (for example, see Kopal 1959 or Wilson & Sofia 1976). Partial eclipses of the star can result in an asymmetric contribution to the star’s rotational velocity to the overall observed radial velocity, leading to a distorted radial velocity curve near the conjunction phases. On May 2, 1995, the secondary star was observed spectroscopically by Bailyn et al. (1995b) as it moved through the spectroscopic phase 0.25 (i.e. as it moved directly behind the disk). The radial velocities from that night (Figure 1) deviate systematically

from the sine curve: just before the phase 0.25, the radial velocities are larger than expected and just after the phase 0.25 the radial velocities are smaller than expected. Stated another way, the residuals of the sine curve fit to the radial velocities (in the sense of “data-model”) are positive just before phase 0.25 and negative just after phase 0.25. As we discussed above, the accretion disk must have had a complex and variable shape to account for some of the features of the 1995 light curves. Modelling the radial velocity curve of GRO J1655-40 is made more difficult by the lack of simultaneous photometry. Nevertheless, the model shown in Figure 10 does produce radial velocity residuals with the correct shape near phase 0.25 (positive just before phase 0.25 and negative just after), but the amplitude of the model residuals was only about 15 km s $^{-1}$, whereas the observed residuals have a much larger amplitude of ≈ 90 km s $^{-1}$. Indeed, we could not explain the large amplitude of the radial velocity residuals from May 2, 1995. Further details of the radial velocity curve models can be found in Orosz (1996).

6. Discussion

The precision of our results for i and Q allow us to determine the masses of the components to unprecedented accuracy for a black hole system (see Table 7). Indeed the formal precision of our results is so high that we expect the true uncertainty of our

TABLE 7
COMPONENT MASSES FOR GRO J1655-40

confidence limit	i (degrees)	Q	M_1 (M_\odot)	M_2 (M_\odot)
1σ	69.42-69.58	2.91-3.07	6.80-7.24	2.20-2.46
3σ	69.00-70.60	2.60-3.45	6.42-7.63	1.86-2.90

results comes from physical effects not included in the models. However, given the good fit between our models and the data, we expect that the systematic errors are also quite small. In the following we discuss the implications of our results for the nature of the secondary star, the radio jet, the evolutionary history of the system, and the outburst mechanism. We will use the parameters listed in Table 7 for the system throughout the following discussion.

6.1. Luminosity and Nature of the Secondary Star

The mass ratio of $Q = 2.99 \pm 0.08$ we found for GRO J1655-40 is the smallest among the seven black hole systems with low mass secondaries. Much larger values of Q have been found for the three systems where the mass ratio has been directly computed via the measurement of the rotational broadening of the secondary star’s absorption lines: $Q = 14.9$ for both A0620-00 (Marsh, Robinson, & Wood 1994) and V404 Cyg (Casares 1995), and $Q = 23.8$ for GS 2000+25 (Harlaftis, Horne, & Filippenko 1996). There are hints that the mass ratio may be extreme in XN Mus91 (Orosz et al. 1994), and GRO J0422+32 (Filippenko, Matheson, & Ho 1995) as well. In GRO J1655-40, we have a way to independently check the value of the mass ratio by comparing the observed luminosity of the secondary star to the luminosity inferred from the model fits. To compute the observed luminosity in V , we adopt a mean V magnitude of $\bar{V} = 17.12$, which is the mean of the model fit to the March, 1996 data, a distance of $d = 3.2 \pm 0.2$ kpc (which is tightly constrained by the kinematics of the radio jets—see Hjellming & Rupen 1995), a disk fraction in V of $5\% \pm 2\%$ (Section 4), and a color excess of $E(B-V) = 1.3 \pm 0.1$ (Horne et al. 1996; Horne private communication 1996). Assuming a visual extinction of $A_v = 3.1E(B-V)$, the observed luminosity in V of

the GRO J1655-40 secondary is $L_{\text{obs}} = 46.6 \pm 13.6 L_\odot$.

The luminosity of the secondary star inferred from the models is easily derived from some simple relations. Given the measured masses and orbital period of the system, we can use Kepler’s Third Law to determine the semi-major axis. Eggleton’s (1983) expression for the effective radius of the Roche lobe then determines the size of the secondary, and the temperature inferred from the spectral type and the Stefan-Boltzmann Law determines the luminosity. Figure 11 shows the computed mass, radius, and luminosity of the secondary star as a function of Q , assuming an inclination of $i = 69.5$ deg, an effective temperature of $T_{\text{eff}} = 6500$ K, and an orbital period of $2^d 62157$. The vertical dashed line in the three panels indicates the value of Q from the best model fit, and the horizontal dashed and dotted lines in the lower panel indicate the observed luminosity of the GRO J1655-40 secondary and its 1σ error. Evidently, models with $Q \lesssim 3.5$ are needed to produce a secondary star with a luminosity large enough to match the observed luminosity of the GRO J1655-40 secondary. Models with larger mass ratios (i.e. $Q \gtrsim 5$) not only produce under-luminous secondary stars, but also provide fits to the data with relatively large χ^2_ν values (Figure 7). The agreement between the luminosity of the secondary calculated from the orbital parameters and that inferred from the known distance and reddening of the source provides a satisfying consistency check for our models.

The observed luminosity of the GRO J1655-40 secondary star is a fairly well-constrained quantity, owing to the fact that the distance is well determined from the kinematics of the radio jets (Hjellming & Rupen 1995) and the amount of interstellar extinction is well determined from high quality UV spectra obtained with the *Hubble Space Telescope* (Horne et al. 1996). The observed spectral type of the star provides a fairly good measure of its effective tem-

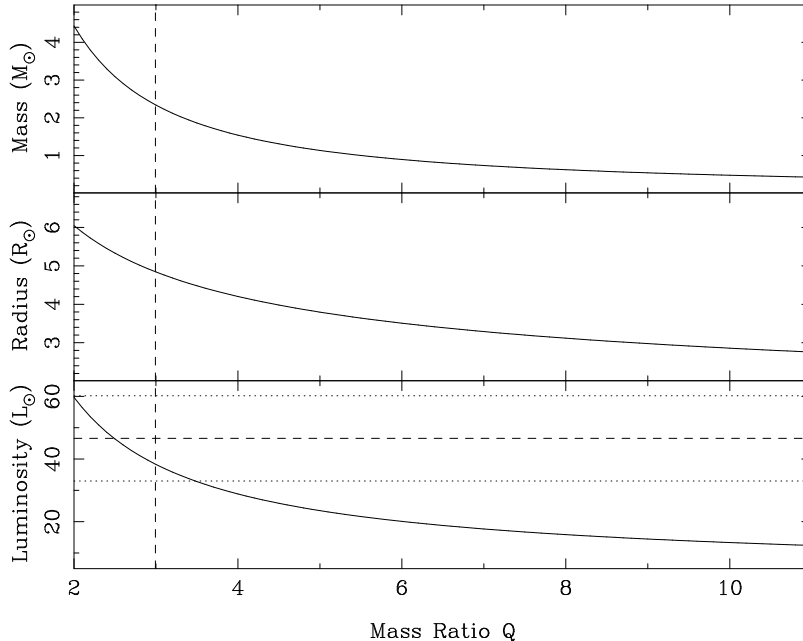


Fig. 11.— The mass (top), radius (middle), and the luminosity (bottom) of the secondary star as a function of the mass ratio Q , assuming $T_{\text{eff}} = 6500$ K, $i = 69.5$ deg, $f(M) = 3.24 M_{\odot}$, and $P = 2^{\text{d}}62157$. The dashed and dotted lines in the lower panel indicate the observed luminosity of the secondary star in GRO J1655-40 and its 1σ error.

perature (e.g. Straižys & Kuriliene 1981), and we adopt $T_{\text{eff}} = 6500 \pm 250$ K. We therefore can accurately place the secondary star of GRO J1655-40 on a Hertzsprung-Russell diagram (Figure 12). Using the Yale Stellar Evolution Code (Guenther et al. 1992) with updated opacities (Iglesias & Rogers 1996), we computed the evolutionary tracks of a $2.1 M_{\odot}$ star, a $2.3 M_{\odot}$ star, and a $2.5 M_{\odot}$ star, assuming a solar metallicity, a hydrogen abundance of 71%, and a mixing length coefficient of 1.7, all typical values for population I stars. These evolutionary tracks are also shown in Figure 12. The secondary star falls very near the track of the $2.3 M_{\odot}$ star, roughly halfway between the main sequence and the giant branch. This provides yet another consistency check for our model. It is interesting to note the radius of the $2.3 M_{\odot}$ star near the position of the secondary: 690 Myr after the zero-age main sequence (ZAMS) the star has a radius of $4.85 R_{\odot}$ (and a temperature of $T_{\text{eff}} = 6813$ K and a luminosity of $L_2 = 45.8 L_{\odot}$); 692 Myr after the ZAMS, the star has a radius of $5.21 R_{\odot}$ (and $T_{\text{eff}} = 6500$ K and $L_2 = 43.8 L_{\odot}$). For $Q = 2.99 \pm 0.08$ and $i = 69.50 \pm 0.08$ deg, the effective radius of the secondary star is $4.85 \pm 0.08 R_{\odot}$ (when given the values

of the orbital period and mass function listed in Table 2). Thus, the observed luminosity, the observed temperature, *and* the inferred radius of the GRO J1655-40 secondary star are all consistent with a $\approx 2.3 M_{\odot}$ *single* star that has evolved $\approx 690 \times 10^6$ years past the ZAMS.

6.2. Inclination of the Radio Jet

Hjellming & Rupen (1995) showed that the relativistic radio jets GRO J1655-40 possessed during late 1994 were inclined 85 ± 2 deg to the line of sight. In addition, the jets were apparently rotating about the jet axis at an angle of 2 deg and with a period of $3^{\text{d}}0 \pm 0^{\text{d}}2$. Our light curve models show that the orbital plane is inclined 69.5 deg to the line of sight. Hence, the jet axis was tilted by 15.5 deg from the normal of the orbital plane. *If* the jet axis was perpendicular to the orbital plane, the 2 deg offset might be explained by a warped accretion disk near the compact object. In this case, the roughly three day periodicity would be closely related to the orbital period of the binary since the orientation of the warp would depend on the orbital phase. However, since the jet

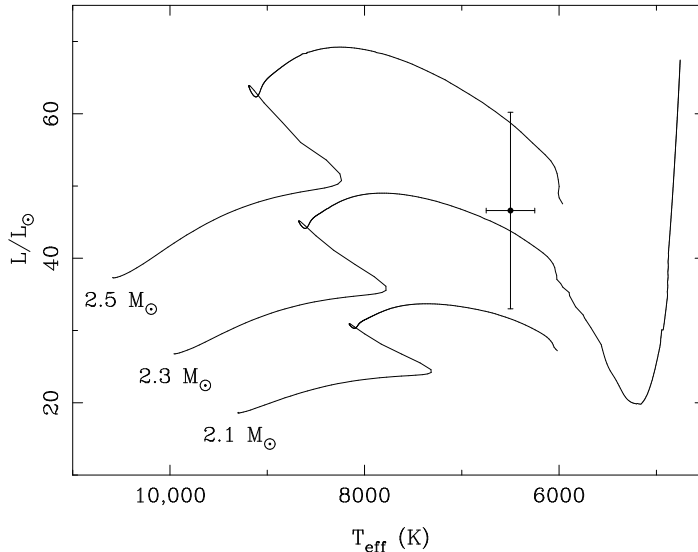


Fig. 12.— A Hertzsprung-Russell diagram showing the position of the secondary star of GRO J1655-40. Evolutionary tracks are shown for a $2.1 M_{\odot}$ star (lower curve), a $2.3 M_{\odot}$ star (middle curve), and a $2.5 M_{\odot}$ star (upper curve), assuming a solar metallicity. In each case, core hydrogen exhaustion takes place just after the tiny loop. The computations of the tracks for the $2.1 M_{\odot}$ star and $2.5 M_{\odot}$ star were stopped short of the giant branch.

axis is *not* perpendicular to the orbital plane, it appears difficult to account for both the 15.5° tilt in the jet axis *and* the 2° rotation about the axis by invoking a simple warp in the inner accretion disk. If the inner disk were warped by 15.5° and the axis of the jet were perpendicular to the warp, we might expect to observe a large precession of jets because the orientation of the warp depends on the orbital phase.

Alternatively, the 15.5° tilt of the jet axis may be a measure of the inclination of the spin axis of the black hole with respect to the orbital plane. In this hypothesis the jet would need to be collimated in some way by the Kerr geometry of the black hole itself. The “wiggles” observed in the jets might be due to the low mass ratio of the system which results in a considerable displacement of the black hole from the center of mass of the binary system: $4.19 \pm 0.19 R_{\odot}$. Thus, if the jet axis is aligned with the black hole, the base of the jets would orbit about the center of mass with a maximum displacement of $\approx 8.4 R_{\odot}$. A highly collimated jet that is being ejected from the very near black hole (along the tilted spin axis) as the black hole orbits the center of mass would have a spiral structure. A more detailed analysis would have to be done to see if the wiggles in the radio jets

with the $3^{\text{d}}0 \pm 0^{\text{d}}2$ periodicity observed by Hjellming & Rupen 1995 can be entirely explained simply by the orbital motion of the black hole. In particular, one would have to consider the physical sizes of the observed wiggles as well as the complicated physical processes taking place inside the jets themselves.

If the tilt in the jet axis comes about because the spin axis of the black hole is tilted, then one needs to explain the misalignment of the spin axis of the black hole and that of the orbital plane. The Monte Carlo simulations of supernovae kicks on neutron star binaries by Brandt & Podsiadlowski (1995) predict that most of the massive stars in these neutron star binaries would have inclined spin axes. If the work of Brandt & Podsiadlowski (1995) can be extended to the black hole systems, it may turn out that a 15.5° tilt in the black hole’s spin axis is not at all unusual.

6.3. Evolution of the System

Despite the pleasing agreement between single star evolutionary models and the observed parameters of the secondary, the evolutionary history of GRO J1655-40 is clearly much more complex than the evo-

lutionary history of a single star (e.g. Webbink 1992; van den Heuvel 1992; Webbink & Kalogera 1994). Webbink & Kalogera (1994) give several conditions for the successful formation of a low mass X-ray binary, some of the conditions being: (i) the progenitor binary must have an extreme mass ratio in order to drive the system to a common envelope *and* the initial binary must be wide enough to survive the common envelope stage; (ii) the post-common-envelope binary must be big enough to accommodate the secondary star within its Roche lobe *and* wide enough to allow the primary to evolve to core collapse; and (iii) the binary system must survive the core collapse. If the conditions stated by Webbink & Kalogera (1994) are met and we are left with a $7 M_{\odot}$ black hole with a $2.3 M_{\odot}$ main sequence companion star in an orbit with a period of about 2.6 days, the subsequent binary evolution will be dominated by the evolution of the secondary star since the timescale for the evolution of that $2.3 M_{\odot}$ star is much shorter than the timescale for the loss of orbital angular momentum (King, Kolb, & Burderi 1996). The orbit is not likely to be left circular after the core collapse, but tidal dissipation will circularize the orbit before the secondary can fill its Roche lobe (Webbink & Kalogera 1994). Once the orbit is circularized, the stellar evolution computations we performed show that on a timescale of order 690 million years, the companion star will evolve off the main sequence and attain a radius, luminosity, and temperature comparable to the secondary star of GRO J1655-40 that we see today. The radius the star attains is roughly the effective radius of the Roche lobe of the secondary star in GRO J1655-40.

GRO J1655-40 stands out among the black hole binaries in that it has a large space velocity (i.e. it has a large γ velocity, see Table 3 and Brandt, Podsiadlowski, & Sigurdsson [1995, hereafter BPS95]). BPS95 argued that GRO J1655-40 may have acquired its velocity as the result of a kick caused by an asymmetry during the initial collapse of the compact object (as is thought to be the case with neutron stars—Brandt & Podsiadlowski 1995; Johnston 1996). BPS95 proposed that the black hole in GRO J1655-40 formed via an intermediate neutron stage, and was then converted into a black hole by additional accretion from the secondary star or through some kind of phase transition in the cooling compact object. This scenario predicts that the final black hole binary system should have a large mass ratio and that the masses of the components would be relatively small

($M_1 \approx 3.6 M_{\odot}$ and $M_2 \approx 0.3 M_{\odot}$). However, our fits to the light curves show that almost the opposite situation is true: the mass ratio Q is relatively close to unity and the masses of the components are relatively large ($M_1 = 7 M_{\odot}$ and $M_2 = 2.3 M_{\odot}$). Therefore, if the compact object passed through an intermediate neutron stage, it would have had to accrete $\gtrsim 5 M_{\odot}$ to attain its present day mass, with the accreted matter presumably coming from the companion star. As we showed above, the position of the secondary star on the Hertzsprung-Russell diagram is consistent with the track of a normal $2.3 M_{\odot}$ star halfway between the main sequence and the giant branch. If the secondary star was once much more massive and it gave up most of its mass to the compact primary, its evolutionary path on the Hertzsprung-Russell diagram could be quite different than that of a normal $2.3 M_{\odot}$ star. Thus, BPS95's proposed scenario of the formation of the black hole in GRO J1655-40 seems to be less viable in view of the large amount of matter the compact object must accrete and the secondary star must give up in order to attain their present-day masses. If the compact object initially formed as a neutron star, it seems likely that a significant amount of material from the supernova itself must have fallen back, thus converting the neutron star into a black hole shortly after its creation. Note that the same supernova kick invoked by BPS95 to explain the large velocity of GRO J1655-40 might also give rise to a substantial tilt in the spin axis of the compact object as discussed in Section 6.2.

6.4. Outburst Mechanism

Recently, King et al. (1996) and van Paradijs (1996) discussed the transient behavior in some low mass X-ray binaries. In general, a system will be transient if the average mass transfer rate \dot{M} is smaller than some critical value. In the case of GRO J1655-40 where the main sequence lifetime of the secondary star is much shorter than the timescale of the shrinkage of the orbit due to angular momentum loss, the average mass loss rate is given by King et al. (1996) as

$$-\dot{M}_2 \approx 4 \times 10^{-10} P_d^{0.93} M_2^{1.47} M_{\odot} \text{ yr}^{-1} \quad (2)$$

where P_d is the orbital period in units of days and where the units of M_2 are solar masses. For GRO J1655-40, $\dot{M}_2 = 3.4 \times 10^{-9} M_{\odot} \text{ yr}^{-1} = 2.16 \times 10^{17} \text{ g s}^{-1}$. This average mass transfer rate is much larger than the average mass transfer rates found in the other six transient black hole systems, which

all have rates around $10^{-10} M_{\odot} \text{ yr}^{-1}$ (van Paradijs 1996). For X-ray heated accretion disks, the critical mass transfer rate is given by

$$\dot{M}_{\text{crit}} \approx 5 \times 10^{-11} M_1^{2/3} P_3^{4/3} M_{\odot} \text{ yr}^{-1} \quad (3)$$

where the units of M_1 are solar masses and where $P_3 = P/(3 \text{ hr})$ (King et al. 1996). For GRO J1655-40, $\dot{M}_{\text{crit}} = 1.1 \times 10^{-8} M_{\odot} \text{ yr}^{-1}$. Thus GRO J1655-40 is *not* expected to be a persistent X-ray source since $\dot{M} < \dot{M}_{\text{crit}}$. It is, however, interesting to note how close GRO J1655-40 is to being a persistent X-ray source. van Paradijs (1996) gives the following relation dividing systems with stable and unstable mass transfer:

$$\log \bar{L}_x = 35.8 + 1.07 \log P(\text{hr}) \quad (4)$$

where \bar{L}_x is the time-averaged X-ray luminosity over one outburst cycle. If a system falls *below* the line defined by Equation 4 in the $P - \bar{L}_x$ plane, then it will be a transient system. If the energy generation rate is $0.2c^2$ per gram of accreted matter (van Paradijs 1996), the averaged mass transfer rate of $= 2.16 \times 10^{17} \text{ g s}^{-1}$ for GRO J1655-40 corresponds to an average X-ray luminosity of $\bar{L}_x = 3.88 \times 10^{38} \text{ erg s}^{-1}$. This is slightly smaller than the value of $\bar{L}_x = 5.31 \times 10^{38} \text{ erg s}^{-1}$ predicted from the relation given by Equation (4). The other six transient black hole systems have average X-ray luminosities that are at least a factor of ten less than the critical X-ray luminosity defined by Equation 4 (see Figure 2 of van Paradijs 1996), which suggests that GRO J1655-40 is likely to have more frequent X-ray outbursts than the other six transient black hole systems. Indeed, there were several additional hard X-ray outbursts after the initial hard X-ray outburst observed July, 1994 (Harmon et al. 1995a), and the soft X-ray outburst observed in late April, 1996 (Remillard et al. 1996a) came less than one year after the sequence of hard X-ray outbursts ended.

7. Summary

Using our database of GRO J1655-40 spectra, we have established much improved values of the orbital period ($P = 2^{\text{d}}62157 \pm 0^{\text{d}}00015$), the radial velocity semiamplitude ($K_2 = 228.2 \pm 2.2 \text{ km s}^{-1}$), the mass function ($f(M) = 3.24 \pm 0.09 M_{\odot}$), and MK spectral type (F3IV to F6IV). Our photometry taken while the system was in true X-ray quiescence shows that light from the distorted secondary star dominates, making

it possible to model the light curves in detail. Our model of a distorted secondary star plus a circular accretion disk provide excellent fits to the light curves taken during true X-ray quiescence. We can add the effects of X-ray heating on the secondary star and fit the general shape of the March 18-25, 1995 *V* and *I* light curves, taken during a period of intense activity in hard X-rays. The best values of the orbital inclination angle i and the mass ratio Q ($i = 69.50 \pm 0.08 \text{ deg}$ and $Q = 2.99 \pm 0.08$) may be combined with the mass function to give, for the first time, a reliable mass for a black hole: $M_1 = 7.02 \pm 0.22 M_{\odot}$. The position of the secondary star on the Hertzsprung-Russell diagram is well determined, and its luminosity, temperature, and radius are all consistent with a $2.3 M_{\odot}$ star ≈ 690 million years into its evolution past the ZAMS. The average mass accretion rate of the system is much larger than the averaged accretion rates of the other transient black hole systems, putting GRO J1655-40 much closer to the threshold where it would be a persistently strong X-ray source.

We are grateful to Sydney Barnes and Dana Diniescu who assisted with the observations, and to the staff of CTIO for the excellent support, in particular Srs. Maurico Navarrete, Edgardo Cosgrove, Maurico Fernandez, & Luis Gonzalez. We thank the CTIO Time Allocation Committee for their flexible scheduling of the spectroscopy run on the 1.5 meter telescope. Alison Sills and Sukyong Yi kindly provided the stellar evolution tracks for us. Mr. Yi also gave us the digitized versions of the standard filter response curves. We thank Nan Zhang for providing us with the BATSE daily flux averages from late March, 1995. We acknowledge useful discussions with Craig Robinson, Jeffrey McClintock, Ronald Remillard, and Richard Wade. Financial support for this work was provided by the National Science Foundation through a National Young Investigator grant to C. Bailyn.

A. Appendix: The Eclipsing Light Curve Code

In this Appendix we describe in detail the code used to model the eclipsing light curve of GRO J1655-40. This program is a modified version of code first written by Yoram Avni (Avni & Bahcall 1975; Avni 1978; see also McClintock & Remillard 1990). We will outline here in detail the basic input physics and approximations used, not to take credit for the work

of Avni and others, but to tell the readers exactly what the code does and how it does it.

A.1. The Potential

Consider a binary system consisting of a visible star of mass M_2 and a compact object of mass M_1 , where the visible star orbits in a circular orbit with a Keplerian angular velocity ω_k . Assume the visible star is also rotating with an angular velocity ω_2 . Following the notation in Avni (1978), we define a rectangular coordinate system with the origin at the center of the visible star, and with the X -axis pointing towards the compact object, and the Z -axis in the direction of $\vec{\omega}_k$. This coordinate system rotates with the visible star. The potential can be written as (Avni 1978)

$$\Psi(X, Y, Z) = -\frac{GM_2}{D} \left[\frac{1}{r_2} + \frac{Q}{r_1} - Qx + \frac{\Omega^2(x^2 + y^2)(1 + Q)}{2} \right] \quad (\text{A1})$$

where D is the separation of the two stars, $Q = M_1/M_2$, $\Omega = \omega_2/\omega_k$, r_1 and r_2 are the distance to the centers of the two stars in units of D , and where x and y , are X and Y in units of D . If $\Omega = 1$ (the visible star is in synchronous rotation), the potential given by Equation (A1) reduces to the standard Roche potential, and the star can be in hydrostatic equilibrium in the rotating frame (Avni 1978). The degree to which the star fills its Roche lobe must be specified—it is usually taken to be 100%.

In practice, it is convenient to adopt units of mass and distance such that the $GM_1/D = 1$. Typically, the star is assumed to be in synchronous rotation, so that $\Omega = 1$, and it is assumed that it completely fills its Roche lobe. Thus the value of the mass ratio Q uniquely determines the function for the potential, and hence the geometry of the Roche surface. Once the value of Q is specified, the visible star is divided into N_ϕ grid points in longitude ϕ , where the points are spaced equally in $\cos \phi$, and $4N_\theta$ grid points in the co-latitude θ , where the points are spaced equally in the angle θ . The value of the potential Ψ and its derivatives are then computed for each point.

A.2. Photometric Parameters

von Zeipel’s Theorem (1924) provides a relationship between the local gravity and the local emergent flux in a tidally distorted star. Proofs of von Zeipel’s

Theorem may be found in Kopal & Kitamura (1968) and Avni (1978). Using von Zeipel’s Theorem, one can show that the light emitted from every point on the photosphere of the star is the same as the light emitted from a plane-parallel atmosphere characterized by the local values of the temperature T_e and gravity g :

$$T_e^4 \propto g. \quad (\text{A2})$$

As a consequence of von Zeipel’s Theorem, the temperature at any point on the star is given by

$$\frac{T(x, y, z)}{T_{\text{pole}}} = \left[\frac{g(x, y, z)}{g_{\text{pole}}} \right]^\beta, \quad (\text{A3})$$

where T_{pole} and g_{pole} are the temperature and gravity at the pole of the star (i.e. the point on the surface of the star where the positive Z -axis emerges). The “gravity darkening exponent” β has two values: 0.25 for stars with radiative atmospheres as shown by von Zeipel (1924), and 0.08 for stars with fully convective envelopes (Lucy 1967). Thus, to specify the temperature $T(x, y, z)$ at every point on the star, one must input the value of T_{pole} . This input temperature is usually taken to be the effective temperature of a field star with a similar spectral type as the star to be modelled. In our model, the surface gravity on each point on the star can be computed from the derivatives of the potential:

$$g(x, y, z) = - \left[\left(\frac{\partial \Psi}{\partial x} \right)^2 + \left(\frac{\partial \Psi}{\partial y} \right)^2 + \left(\frac{\partial \Psi}{\partial z} \right)^2 \right]^{1/2} \quad (\text{A4})$$

e.g. (Zhang, Robinson, & Stover 1986).

Once the temperature is computed for each surface point, Planck’s function is used to approximate the relationship between the temperature and the monochromatic intensity

$$I(\lambda) \propto \left[\exp \left(\frac{hc}{k\lambda T_e} \right) - 1 \right]^{-1}, \quad (\text{A5})$$

where h , c , and k are the usual physical constants. The star appears darker near its limb, a phenomenon referred to as limb darkening. The code presently uses a standard linear limb darkening law expressed as

$$I(\lambda) \propto 1 - u(\lambda) + u(\lambda) \cos \mu, \quad (\text{A6})$$

where μ is the angle between the surface normal and the line of sight. The values of the coefficient $u(\lambda)$ are taken from standard tables computed from model

atmospheres (e.g. Al-Naimiy 1978). The reader is referred to Kopal (1959), Kopal & Kitamura (1968), and Avni (1978) for more discussions on these approximations.

A.3. Integration of the Flux from the Star

Let $L(\lambda)$ be the radiation emitted by the star at the wavelength λ as seen at a great distance. If $I(\lambda, x, y, z)$ is the intensity of the light at a surface point, the total observed flux is given by

$$L(\lambda) = \int I(\lambda, x, y, z) \cos \gamma ds, \quad (\text{A7})$$

where γ is the angle of foreshortening, ds is the surface element, and where the integration is to be done over the entire visible surface of the star (Kopal & Kitamura 1968).

To carry out the numerical integration of the flux, some quantities need to be defined. First, each point on the surface has direction cosines:

$$\begin{aligned} \ell_x &= \cos \phi \\ \ell_y &= \sin \phi \cos \theta \\ \ell_z &= \sin \phi \sin \theta. \end{aligned} \quad (\text{A8})$$

The element of the surface area $dS(x, y, z)$ is given by

$$dS(x, y, z) = \frac{R^2 \Delta \phi \Delta \theta}{\sigma(x, y, z)} \quad (\text{A9})$$

where $R^2 = x^2 + y^2 + z^2$, $\Delta \phi$ and $\Delta \theta$ are the grid sizes in longitude and co-latitude, respectively, and where

$$\begin{aligned} \sigma(x, y, z) &= -\frac{\ell_x}{g(x, y, z)} \left(\frac{\partial \Psi(x, y, z)}{\partial x} \right) \\ &\quad - \frac{\ell_y}{g(x, y, z)} \left(\frac{\partial \Psi(x, y, z)}{\partial y} \right) \\ &\quad - \frac{\ell_z}{g(x, y, z)} \left(\frac{\partial \Psi(x, y, z)}{\partial z} \right). \end{aligned} \quad (\text{A10})$$

Next, let Θ be the orbital phase of the observation (where $\Theta = 0$ corresponds to the time of the closest approach of the visible star) and let i be the inclination of the orbit ($i = 90$ deg for an orbit seen edge-on). The foreshortening $\Gamma(x, y, z)$ of a particular point on the star depends on the phase of the observation, the inclination, and on the (x, y, z) coordinates of the point:

$$\Gamma(x, y, z) = -\frac{1}{g(x, y, z)} \left(\sin i \cos \Theta \frac{\partial \Psi(x, y, z)}{\partial x} \right)$$

$$\begin{aligned} &+ \frac{1}{g(x, y, z)} \left(\sin i \sin \Theta \frac{\partial \Psi(x, y, z)}{\partial y} \right) \\ &+ \frac{1}{g(x, y, z)} \left(\cos i \frac{\partial \Psi(x, y, z)}{\partial z} \right). \end{aligned} \quad (\text{A11})$$

If the ‘‘projection factor’’ $\Gamma(x, y, z) < 0$, then that particular point is not visible. At each phase, the flux elements from the visible points (i.e. those with $\Gamma(x, y, z) > 0$) are simply summed up:

$$L_{\text{star}}(\Theta, \lambda) = \sum_{i=1}^{N_\phi} \sum_{j=1}^{4N_\theta} I(\lambda, x, y, z) \Gamma(x, y, z) dS(x, y, z), \quad (\text{A12})$$

where each pair of (i, j) indices are associated with a specific (x, y, z) point on the star. In practice, the above sum in Equation (A12) converges effectively for $N_\phi \geq 40$ and $N_\theta \geq 14$.

So far, Equations (A1) through (A12) describe the basic input physics and mathematics of the original Avni code (Avni & Bahcall 1975; Avni 1978). This code models the light curve due to a single Roche lobe filling star. Extra sources of light such as light due to X-ray heating effects are not taken into account in the Avni code. To summarize the model so far, the user specifies the degree to which the star fills its Roche lobe (usually 100%), the value of the mass ratio Q , and the rate of the star’s rotation (usually $\Omega = 1$ for synchronous rotation). These three quantities define the shape of the surface of the star. Then the user must specify the polar temperature of the star T_{pole} , the gravity darkening exponent β (either 0.25 or 0.08 depending on whether the star has a radiative envelope or a convective envelope), and the linearized limb darkening coefficient $u(\lambda)$ appropriate for the star in question in order to compute the temperatures over the surface of the star. Once the temperatures are known, the Planck function and a linearized limb darkening law are used to compute the intensities over the surface. Finally, after the orbital phase and the inclination of the orbit are specified, the total observed flux can be computed.

A.4. The Addition of an Accretion Disk

To make the basic Avni code more realistic, we added an accretion disk to the code. Following Zhang et al. (1986), the disk is flattened cylinder centered on the (invisible) compact object. The plane of the orbit bisects the disk in the z -direction. The disk is assumed to be completely optically thick, so that we can only see light from its surface and so that anything

behind the disk is completely eclipsed. The face of the disk is divided up into several grids equally spaced in the polar coordinates (r, α) . The outer radius of the disk r_d is scaled to a user specified fraction of the effective Roche lobe radius of the primary and the inner radius r_i is set to a very small number (typically 0.005). Eggleton’s (1983) approximation is used to compute the effective Roche lobe radius. The thickness of the disk at the outer edge is $z_d = 2r_d \tan \beta_{\text{rim}}$. With the exception of user-defined “hot-spots”, the temperature of the disk does not vary with the azimuth angle. The radial distribution of the temperature across the face of the disk is given by

$$T(r) = T_{\text{disk}}(r/r_d)^\xi, \quad (\text{A13})$$

where T_{disk} is the user specified temperature at the outer edge of the disk. For a steady-state, optically thick, viscous accretion disk, the power law exponent $\xi = -0.75$ (Pringle 1981). As before, Planck’s function is used to approximate the relationship between the temperature of a point on the surface of the disk and the monochromatic intensity $I_{\text{disk}}(\lambda, r, \alpha)$ of that point.

Recently Diaz, Wade, & Hubeny (1996) discussed the importance of including corrections for limb darkening in models of disk spectra. Limb darkening is important for disks since the limb darkening corrections depend on the temperature (and hence the radius in our model) and on the effective wavelength. Therefore the slope of a blackbody disk’s spectrum will be in error if no limb darkening corrections are made. An important result of the work of Diaz et al. (1996) is that the limb darkening law in the optically thick rings of their accretion disk models is very similar to the limb darkening law in a stellar atmosphere. As a result, one may use the same linearized limb darkening coefficients for disks that one uses for stars. We therefore have

$$I_{\text{disk}}(\lambda, r, \alpha) \propto 1 - u_{\text{disk}}(\lambda, T(r)) + u_{\text{disk}}(\lambda, T(r)) \cos i \quad (\text{A14})$$

where the values of $u_{\text{disk}}(\lambda, T(r))$ are interpolated from tables given by Wade & Rucinski (1985).

The foreshortening angle of the normal of a surface element on the face of the disk is simply $\cos i$. In the absence of eclipses, the observed flux from the face of

the accretion disk is:

$$L_{\text{disk}}(\Theta, \lambda) = \sum_{i=1}^{N_r} \sum_{j=1}^{N_\alpha} I_{\text{disk}}(\lambda, r, \alpha) (\cos i) r \Delta r \Delta \alpha, \quad (\text{A15})$$

where N_r and N_α are the number of grid points in radius and azimuth, respectively, where Δr and $\Delta \alpha$ are the grid spacings in radius and azimuth, and where each pair of (i, j) indices are associated with a specific (r, α) point on the disk.

To handle the situations where the disk has a substantial thickness, light from the rim is also accounted for. The rim is divided into 11 grid points in the z direction, and N_α grid points in azimuth. The temperature of the rim is T_{rim} , and the intensities of each rim point are found using Planck’s function. If the azimuth angle α is measured from the X -axis, then the foreshortening factor $\Gamma_{\text{rim}}(\alpha)$ of a point on the rim at the orbital phase Θ is

$$\Gamma_{\text{rim}}(\alpha) = \sin i \cos(\alpha + \Theta). \quad (\text{A16})$$

If $\Gamma_{\text{rim}}(\alpha) < 0$, the point is hidden. A limb darkening correction is made for the edge surface elements based on the value of $\Gamma_{\text{rim}}(\alpha)$:

$$I_{\text{rim}}(\lambda, \alpha) \propto 1 - u_{\text{disk}}(\lambda, T_{\text{disk}}) + u_{\text{disk}}(\lambda, T_{\text{disk}}) \Gamma_{\text{rim}}(\alpha) \quad (\text{A17})$$

The total flux from the rim is found by summing the intensities of all visible points:

$$L_{\text{rim}}(\Theta, \lambda) = \sum_{i=1}^{11} \sum_{j=1}^{N_\alpha} I_{\text{rim}}(\lambda, \alpha) \Gamma_{\text{rim}}(\alpha) \Delta z \Delta \alpha, \quad (\text{A18})$$

where Δz is the step size in the Z direction, and where each pair of (i, j) indices are associated with a specific (z, α) point on the rim.

Hot spots can be added to the disk. The spots are confined to radii $r_{\text{cut}} \leq r \leq r_d$ and azimuth angles $\alpha_1^i \leq \alpha \leq \alpha_2^i$, where at the moment $i = 0$ (no spots), 1 or 2. The temperature of the spot T_{spot} is added to the temperature $T(r, \alpha)$ of each point on the disk rim and face that lies inside the spot boundaries. The intensities of each point are computed as before and the integrations are carried out as before (e.g. Equations (A15) and (A18)).

In the absence of eclipses, the total observed flux from the star and the disk is

$$L_{\text{total}}(\Theta, \lambda) = L_{\text{star}}(\Theta, \lambda) + L_{\text{disk}}(\Theta, \lambda) + L_{\text{rim}}(\Theta, \lambda). \quad (\text{A19})$$

A.5. The Addition of Eclipses

In the case where the inclination angle i is large enough to allow for eclipses, the procedure for computing the light curves must be modified slightly. First, the intensities of each point on the star, disk face, and disk rim are computed from the list of input parameters. We can determine which body is in front of the other body from the orbital phase Θ —the star will obviously be closer than the disk for $0 \text{ deg} \leq \Theta \leq 90 \text{ deg}$ or for $270 \text{ deg} \leq \Theta \leq 360 \text{ deg}$ and the other way around for $90 \text{ deg} \leq \Theta \leq 270 \text{ deg}$. The integration of the flux elements over the visible surface of the object in front is carried out as before. Then, all points on the edge of the body in front (i.e. its horizon) are determined and are projected onto the plane of the sky. The horizon of the eclipsing body defines some polygon on the plane of the sky. Then, as the integration of the flux elements of the body in back is carried out, each potentially visible point is projected onto the plane of the sky and checked to see if it falls inside the horizon of the eclipsing body. If the point is eclipsed, it is not included in the integration. Once all of the visible points are included in the integrations, the total observed flux is found as before (Equation (A19)).

A.6. The Addition of X-ray Heating

If the secondary star intercepts a large amount of flux from the other body (either X-ray heating from the vicinity of the compact object or optical light from the disk), there may be a large amount of reprocessed radiation. The irradiating flux can strongly alter the distribution of temperatures across the face of the star. A rigorous treatment of these “reflection effects” requires difficult and time-consuming computations (e.g. Kopal 1959; Wilson & Devinney 1971). Following Zhang et al. (1986), we will use a simplified treatment of the heating effects. We will consider only heating of the star by X-ray heating, and not the heating of the disk by the star. For simplicity, all of the irradiating flux F_{irr} due to the X-ray heating is assumed to come from the center of the compact object.

The *total* energy in X-rays intercepted by the Roche lobe filling secondary star does not depend on the scale of the orbit since the surface area of Roche lobe filling star facing the X-ray source is proportional to the square of the orbital separation. However, the change in the star’s atmosphere caused by the X-ray

heating *does* depend on the size of the orbit. As the distance between the star and the X-ray source is increased, each square centimeter on the star’s surface receives less energy in X-rays. The change in the local temperature depends on the amount of absorbed X-ray flux per unit area. So to find the magnitude of the irradiating flux seen by each point on the secondary, the X-ray luminosity of the X-ray source L_x (in ergs s^{-1}) and the physical size of the orbit must be specified. The code uses the mass function $f(M)$ and the orbital period P to find the scale of the orbit.

The distance d (in units of the orbital separation) between each point on the face of the star and the X-ray source can be found

$$d(x, y, z) = (1 + z^2 + R^2 - 2R\ell_x), \quad (\text{A20})$$

where ℓ_x is one of the direction cosines (Equation (A8)), and where $R^2 = x^2 + y^2 + z^2$. The foreshortening factor $\Gamma_{\text{X-ray}}(x, y, z)$ is given by

$$\Gamma_{\text{X-ray}}(x, y, z) = \frac{x(1-x) - y^2 + z^2}{Rd}, \quad (\text{A21})$$

where $\Gamma_{\text{X-ray}}(x, y, z) < 0$ indicates that the point on the star cannot see the X-ray source. The amount of X-ray flux each surface element intercepts is

$$F_{\text{irr}}(x, y, z) = \left(\frac{L_x}{4\pi a^2 d(x, y, z)^2} \right) \Gamma_{\text{X-ray}}(x, y, z). \quad (\text{A22})$$

The modified temperature of each surface point that can see the X-ray source is given by

$$T_{\text{X-ray}}^4(x, y, z) = T_{\text{pole}}^4 \left(\frac{g(x, y, z)}{g_{\text{pole}}(x, y, z)} \right)^{4\beta} + \frac{WF_{\text{irr}}}{\sigma} \quad (\text{A23})$$

where W is the albedo, and σ is the Stefan-Boltzmann constant (Zhang et al. 1986). The albedo W is not very well determined, and it is usually set to 0.5 (see Zhang et al. 1986).

In the cases there the disk has a substantial thickness, some points on the face of the star may be below the rim of the disk as seen from the compact object. These points would not receive any X-ray flux from the compact object and hence their temperatures would not change. It is easy to find the angle above the plane that a point on the face of the star has (as seen from the compact object):

$$\Phi(x, y, z) = \arctan \left(\frac{z}{(1-x)\cos\eta} \right) \quad (\text{A24})$$

where $\eta = \arctan(y/x)$. This angle $\Phi(x, y, z)$ is compared to the angle of the rim β_{rim} to see whether or not the point on the star is blocked by the disk. If $\beta_{\text{rim}} > \Phi(x, y, z)$, the point cannot see the X-ray source.

Once each point on the face of the star has been assigned a new temperature based on the amount of X-ray flux it sees, the intensities and the fluxes are found following the procedures outlined above. The net result is that the points on the star facing the X-ray source are brighter than they would otherwise be because the temperatures were raised.

A.7. Filter Response Curves

We compute the total flux $L_{\text{total}}(\Theta, \lambda)$ at each phase Θ for several values of the effective wavelength λ using limb darkening coefficients $u(\lambda)$ interpolated from tables given by Wade & Rucinski (1985). This model “spectrum” is integrated with the standard *UBVRI* filter response curves (Bessell 1990) to produce model *UBVRI* magnitudes. In this way we can perform simultaneous fits to light curves in several colors. In the case of GRO J1655-40, there is a large amount of reddening in the light curves. Rather than attempting to include the reddening correction in the fits, we instead fit the models to the normalized *BVRI* data. In this way, the error of $E(B - V)$ does not enter into the analysis. We do, however, lose the absolute color information contained in the model.

A.8. Light Curve Fitting and Error Analysis

We first compute a grid of models and χ^2 fits to the data using a wide range of parameters spaced in uniform steps. Then several sets of parameters that produce low χ^2 values are chosen and are used as starting points for an optimization routine based on the GRIDLS program given in Bevington (1969). This “grid search” method was picked because it is easy to implement and it does not require the computation of derivatives. After several runs with different starting points, the set of parameters that gives the lowest overall χ^2 fit to the data is chosen. By using several different starting points for the optimization routine, we can be reasonably sure that we have found the global minimum of χ^2 , rather than a local minimum.

We use three methods to estimate the statistical errors on the fitted parameters. The first one is a “bootstrap” method (Press et al. 1992). Artificial data sets are constructed from the original data set and the ex-

act fitting procedures which were used on the original data are used on the artificial data. The 1σ errors on the parameters are then derived from the distributions of the fitted parameters from the many artificial data sets. The second technique we use is outlined by Zhang et al. (1986). Basically the 1σ error on a fitted parameter a_0 is found by fixing the value of that parameter at a new value $a'_0 = a_0 + \delta$ and finding the values of the rest of the parameters a_1 through a_n that minimize χ^2 . The probable error of a_0 is related to the change in χ^2 and to δ . We typically use two or three different values of δ (1%, 2%, and 3% of the value of the parameter) and average the resulting values of σ . Finally, the GRIDLS program given in Bevington (1969) also provides error estimates based on the shape of the chi-square hypersurface near the minimum. We used primarily the errors derived from the bootstrap method. We stress here that the errors estimated are only internal statistical errors, and not systematic errors which we have no easy way to compute.

REFERENCES

- Al-Naimiy, H. M. 1978, *Ap&SS*, 53, 181
- Avni, Y., & Bahcall, J. N. 1975, *ApJ*, 197, 675
- Avni, Y. 1978, in “Physics and Astrophysics of Neutron Stars and Black Holes,” eds. R. Giacconi & R. Ruffini (Amsterdam: North-Holland), 42
- Bailyn, C. D., et al. 1995a, *Nature*, 374, 701
- Bailyn, C. D., Orosz, J. A., McClintock, J. E., & Remillard, R. A. 1995b, *Nature*, 378, 157
- Bessell, M. S. 1990, *PASP*, 102, 1181
- Bevington, P. R. 1969, “Data Reduction and Error Analysis for the Physical Sciences,” (New York: McGraw-Hill Book Company)
- Brandt, W. N., & Podsiadlowski, Ph. 1995, *MNRAS*, 274, 461
- Brandt, W. N., Podsiadlowski, Ph., & Sigurdsson, S. 1995, *MNRAS*, 277, L35 (BPS95)
- Campbell-Wilson, D., & Hunstead, R. 1994, *IAU Circular # 6052*
- Campbell-Wilson, D., & Hunstead, R. 1996, *IAU Circular # 6410*
- Casares, J. 1995, to be published in *Proc. IAU Colloquium 158 “Cataclysmic Variables and Related Objects”*, 26-30 June 1995, Keele University, UK

- Chevalier, C., & Ilovaisky, S. A. 1993, *A&A*, 269, 301
- Diaz, M. P., Wade, R. A., & Hubeny, I. 1996, *ApJ*, 459, 236
- Eggleton, P. E. 1983, *ApJ*, 268, 368
- Filippenko, A. V., Matheson, T., & Ho. L. C. 1995a, *ApJ*, 455, 614
- Guenther, D. B., Demarque, P., Kim, Y.-C., & Pinsonneault, M. H. 1992, *ApJ*, 387, 372
- Harlaftis, E. T., Horne, K., & Filippenko, A. V., *PASP*, in the press
- Harmon, B. A., et al. 1995a, *Nature*, 374, 703
- Harmon, B. A., et al. 1995b, *IAU Circular #6205*
- Haswell, C. A., Robinson, E. L., Horne, K., Stiening, R. F., & Abbott, T. M. C. 1993, *ApJ*, 411, 802
- Haswell, C. A. 1996, in “Compact Stars in Binaries,” *IAU Symposium #165*, eds J. van Paradijs, E. P. J. van den Heuvel, & E. Kuulkers, page 351
- Hellier, C., & Mason, K. O. 1989, *MNRAS*, 239, 717
- Hjellming, R. M., & Rupen, M. P. 1995, *Nature*, 375, 464
- Hjellming, R. M., & Rupen, M. P. 1996, *IAU Circular #6411*
- Horne, K., et al. 1996, *IAU Circular #6406*
- Iglesias, C. A., & Rogers, F. J. 1996, *ApJ*, 464, 943
- Inoue, H., Nagase, F., Ishida, M., Sonobe, T., & Ueda, Y. 1994, *IAU Circular #6063*
- Johnston, H. M. 1996, in “Evolutionary Processes in Binary Stars,” eds R. A. M. J. Wijers, M. B. Davies, & C. A. Tout, (Kluwer Academic Publishers, Dordrecht), page 385
- King, A. R., Kolb, U., & Burderi, L. 1996, *ApJ*, 464, L127
- Kopal, Z. 1959, “Close Binary Systems”, *The international Astrophysics Series Vol. 5* (New York: Chapman Hill & John Wiley)
- Kopal, Z., & Kitamura, K. 1968, *Advances in Astronomy and Astrophysics*, 6, 125.
- Lucy, L. B. 1967, *ZAp*, 65, 89
- Lucy, L. B., & Sweeney, M. A. 1971, *AJ*, 76, 544
- Marsh, T. R., Robinson, E. L., & Wood, J. H. 1994, *MNRAS*, 266, 137
- McClintock, J. E., & Remillard, R. A. 1986, *ApJ*, 308, 110
- McClintock, J. E., & Remillard, R. A. 1990, *ApJ*, 350, 386
- Morgan, W. W., & Keenan, P. C. 1973, *ARA&A*, 11, 1973
- Orosz, J. A., Bailyn, C. D., Remillard, R. A., McClintock, J. E., & Foltz, C. B. 1994, *ApJ*, 436, 848
- Orosz, J. A., Bailyn, C. D., McClintock, J. E., & Remillard, R. A. 1996, *ApJ*, to appear September 1, 1996
- Orosz, J. A. 1996, Ph.D. Thesis, Yale University
- Press, W. H., Teukolsky, S. A., Vetterling, W. T., & Flannery, B. P. 1992, “Numerical Recipes in Fortran: The Art of Scientific Computing,” second edition, (Cambridge: Cambridge University Press)
- Pringle, J. E. 1981, *ARA&A*, 19, 137
- Remillard, R. A., et al. 1996a, *IAU Circular #6393*
- Remillard, R. A., Orosz, J. A., McClintock, J. E., & Bailyn, C. D. 1996b, *ApJ*, 459, 226
- Robinson, C., et al. 1996, *ApJ*, submitted
- Stetson, P. B. 1987, *PASP*, 99, 191
- Stetson, P. B., Davis, L. E., & Crabtree, D. R. 1991, in “CCDs in Astronomy,” ed. G. Jacoby, *ASP Conference Series, Volume 8*, page 282
- Stetson, P. B. 1992a, in “Astronomical Data Analysis Software and Systems I,” eds D. M. Worrall, C. Biemesderfer, & J. Barnes, *ASP Conference Series, Volume 25*, page 297
- Stetson, P. B. 1992b, in “Stellar Photometry—Current Techniques and Future Developments,” *IAU Coll. 136*, eds C. J. Butler, & I. Elliot, Cambridge University Press, Cambridge, England, page 291
- Straizys, V., & Kuriliene, G. 1981, *Ap&SS*, 80, 353
- Tingay, S. J., et al. 1995, *Nature*, 374, 141
- Tonry, J. & Davis, M. 1979, *AJ*, 84, 1511
- van den Heuvel, E. P. J. 1992, in “X-ray Binaries and Recycled Pulsars,” eds E. P. J. van den Heuvel & S. A. Rappaport, Kluwer Academic Publishers, Dordrecht, The Netherlands, page 233
- van der Hooft, F., et al. 1996, *MNRAS*, submitted
- van Paradijs, J. 1996, *ApJ*, 464, L139
- von Zeipel, H. 1924, *MNRAS*, 84, 665
- Wade, R. A., & Rucinski, S. M. 1985, *A&AS*, 60, 471
- Wagner, R. M., Kreidl, T. J., Howell, S. B., & Starfield, S. G. 1992, *ApJ*, 401, L97

- Webbink, R. F. 1992, in “X-ray Binaries and Recycled Pulsars,” eds. E. P. J. van den Heuvel & S. A. Rappaport, Kluwer Academic Publishers, Dordrecht, The Netherlands, page 269
- Webbink, R. F., & Kalogera, V. 1994, in “The Evolution of X-ray Binaries”, AIP Conference Proceedings #308, eds. S. S. Holt & C. S. Day, page 321
- Wilson, R. E., & Sofia, S. 1976, ApJ, 203, 182
- Wilson, R. E., & Devinney, E. J. 1971, ApJ, 182, 539
- Wilson, C. A., Harmon, B. A., Zhang, S. N., Paciesas, W. S., & Fishman, G. J. 1995, IAU Circular #6152
- Zhang, E. -H., Robinson, E. L., & Stover, R. E. 1986, ApJ, 305, 740
- Zhang, S. N., et al. 1994, IAU Circular #6046